frontiers in Materials

REVIEW
published: 28 June 2016
doi: 10.3389/fmats.2016.00029

Recent Progress in Multifunctional Graphene Aerogels

*Moumita Kotal, Jaehwan Kim, Junghwan Oh and Il-Kwon Oh**

Department of Mechanical Engineering, Korea Advanced Institute of Science and Technology, Daejeon, South Korea

Two dimensional (2D) graphene has become one of the most intensively explored carbon allotropes in materials science owing to attractive features like its outstanding physicochemical properties. In order to further practical applications, the fabrication of self-assembled 2D individual graphene sheets into 3D graphene aerogels (GAs) with special structures and novel functions is now becoming essential. Moreover, GAs are ideal as supports for the introduction of nanoparticles, polymers, and functional materials to further enhance their applications in broad areas. GAs have light weight, large surface area, good compressibility, extensibility, and high electrical conductivity. They have been used as efficient electrodes for batteries, in supercapacitors, and in sensors and actuators. This critical review mainly addresses recent progress in the methods used for their synthesis, their properties, and applications for energy storage, and in sensors and actuators. Furthermore, to assist advanced research for practical applications of these emerging materials, the technical challenges are discussed, and future research directions are proposed.

Keywords: graphene, aerogel, supercapacitor, sensors and actuators, energy storage materials

OPEN ACCESS

Edited by:
Davide Ricci,
Istituto Italiano di Tecnologia, Italy

Reviewed by:
Thiagarajan Soundappan,
Washington University in St. Louis, USA
Feng Du,
Case Western Reserve University, USA

****Correspondence:***
Il-Kwon Oh
ikoh@kaist.ac.kr

Specialty section:
This article was submitted to Carbon-Based Materials, a section of the journal Frontiers in Materials

Received: *29 February 2016*
Accepted: *13 June 2016*
Published: *28 June 2016*

Citation:
Kotal M, Kim J, Oh J and Oh I-K (2016) Recent Progress in Multifunctional Graphene Aerogels. Front. Mater. 3:29. doi: 10.3389/fmats.2016.00029

INTRODUCTION

Graphene, a robust two-dimensional (2D) sheet-like allotrope of carbon, is an extensively studied nano material owing to its distinctive combination of thermal, electrical, and mechanical properties (Novoselov et al., 2005; Li and Kaner, 2008). Flourishing nanotechnology and incredible innovations in research on graphene have indicated prodigious potential for its varied application in the area of photonics, electronics, energy storage and generation, sensors, bio-applications, and the environment. These fascinating properties endow it with great potential as a unique molecular building block toward the construction of macroscopic 3D monoliths. Therefore, the current focus is on assembly of 2D graphenes into 3D architectural forms of new bulk materials. These materials should integrate the fascinating properties of discrete nanostructures with the unique features of porous networks, like ultralight weight, high specific surface area, hierarchical microstructure, excellent electrical conductivity, and mechanical strength (Li and Shi, 2012; Nardecchia et al., 2013). Such assembly of graphene into 3D forms is known to be one of the most favorable approaches for "bottom-up" nanotechnology and has become one of the most promising research areas during the last 5 years. In the past few years, a number of approaches have been established to fabricate 3D interconnected structures of graphene (e.g., ice template, wet chemistry assembly, self-gelation, freeze casting, chemical vapor deposition (CVD), and *in situ* unzipping of carbon nanotubes sponge) (Min et al., 2013; Fang et al., 2015). For most of the methods, freeze drying or supercritical drying is essential to inhibit capillary-force-driven structural collapse of graphene 3D networks

during drying. Both drying techniques produced different pore characteristics: macropores and mesopores. However, relative to the freeze-dried method, the supercritical CO_2 drying offered many more mesopores with ample volume (2.48 cm^3 g^{-1}). Actually, during the freeze drying process, many mesopores fused together to form macropores, a process prompted by the growing of ice crystals. These approaches generally provide ultralight bulk materials with various types of microstructures ranging from isotropic, nanoporous assemblies to ordered, macroscopic cellular networks. Therefore, in this respect, 3D macroscopic assemblies exhibit several inherent merits, like more paths for easier access and diffusion of ions and molecules, large surface area, great mechanical strength, high electrical conductivity and superior thermal, chemical, or electrochemical stability. They also exhibit responsiveness to stimuli, ample oxygen-containing functional groups, and conjugated domains, which are useful in wide applications. Therefore, such 3D graphene aerogels (GAs) hold technological promise toward a wide range of applications like energy storage, sensors, catalyst supports, actuators, and environmental remediation. Interestingly, compared with carbon nanotube based 3D architectures, graphene-based 3D materials offer more advantages, including easy preparation, high efficiency, and economical devices (Nardecchia et al., 2013).

Although, several reviewers highlighted the applications and synthesis of 3D graphene-based materials, a review from detailed descriptions of GA synthesis and their applications for energy storage (supercapacitors and batteries), sensors, and actuators has not been done. In this context, this review article has presented the recent progress related to the synthesis of innovative 3D GAs for their applications in the fields of energy storage, sensors, and actuators. Moreover, in order to inspire more exciting developments in future, challenges and outlook are offered.

SYNTHESIS, PROPERTIES, AND STRUCTURES OF GRAPHENE AEROGELS

Due to the unique structures and appealing properties of graphene-based 3D materials, continuous efforts have been carried out to fabricate 3D-Graphene-based materials with well-ordered structures. In this section, along with the construction techniques and properties, the resulting 3D-G structures are reported.

Self-Assembly Methods, Structures, and Properties

Direct Self-Assembly of Graphene Oxide

Self-assembly of GO sheets is the most effective method for the design of 3D-Gs. Actually, in stable GO suspension, individual GO sheets are well dispersed owing to their electrostatic repulsion from the functional groups on GO sheets, and to van der Waals attraction from the basal planes of GO sheets. The gelation of a GO suspension starts when the balance between these forces is lost, leading to interconnection of the GO sheets with each other to form hydrogel, which after freeze drying generates 3D porous architecture. Therefore, the formation of graphene hydrogel is determined by various supramolecular interactions like van der Waals forces, π–π stacking interactions, hydrogen bonding, electrostatic interactions, and dipole interactions of graphene sheets (Chabot et al., 2014). Importantly, the presence of π–π stacking interactions of graphene sheets was confirmed due to the smaller interlayer spacing of the hydrogel (3.76 Å) compared to that of GO (6.94 Å). This was caused by recovery of π-conjugation of the GO sheets upon gelation. Chemically converted graphene was found to self-gelate without any additional gelators if the dispersion exceeded a certain concentration (Li et al., 2008). The hydrophilic, oxygen-containing groups on the GO surface initiated hydration-induced repulsive forces. Along with these forces, hydrophobic interaction between basal planes, and H-bond interaction between the functional groups, contributed to the self-assembly of GO suspensions. In addition, the critical gel concentration (CGC) is also an important factor for the gelation of GO suspensions. Qin et al. reported CGC of GO was 30 mg/mL during the dispersion of GO by sonication (Qin et al., 2012). However, hydrogel was also formed even when the CGC of GO was 0.075–0.125 mg/mL – but the mechanical strength of the aerogel was weak. Therefore, it is difficult to simultaneously achieve low density and high mechanical strength. In this context, self-assembly using hydrothermal and chemical reductions are the most popular techniques to form hydrogels. Wu et al. (2012a,b,c,d) prepared graphene oxide aerogel using the self-assembly approach followed by hydrogen reduction of graphene oxide aerogel to develop GA. This GA possessed high surface area and large pore size. Gelation of a GO suspension takes place by self-assembly of GO sheets through various physical treatments like direct freeze-drying, hydrothermal treatment, electrochemical deposition, controlled centrifugation/filtration, or light/temperature initiation. The surface tension within the gel resists the flow of liquid that might disrupt the bonds. There are several techniques for initiating the gelation of GO suspensions, for example, changing the pH value of dispersed GO solution, introducing cross-linkers, and employing chemical reactions.

Hydrothermal-Reduction-Induced Self-Assembly

Xu et al. first developed a one-step hydrothermal process to form self-assembled graphene hydrogel, as shown in **Figures 1A–F** (Xu et al., 2010). It was mechanically strong, electrically conductive, thermally stable, and exhibited high specific capacitance. It could support 100 g of weight with little deformation and the corresponding GO concentration was lower (2 mg mL^{-1}) than that (30 mg mL^{-1}) reported by Qin et al. (2012) for direct gelation. The strong graphene skeleton is responsible for the greater mechanical strength than that exhibited by conventional hydrogels. Most importantly, the GO concentration is another factor affecting the morphology and properties of 3D-G. Interestingly, with increasing hydrothermal reaction time, the degree of reduction of the GO increased, along with improvement of the corresponding storage modulus, compressive elastic modulus, and electrical conductivity (Xu et al., 2010). However, the BET surface area and total pore volume of the GA was reduced after drying, as reported by Nguyen et al. (2012). Therefore, 3D-G could be employed as perfect framework to make hierarchical macro- and mesoporous structures by the addition of other functional guests. Li et al. (2012) used tri-isocyanate for the reinforcement of GAs, which

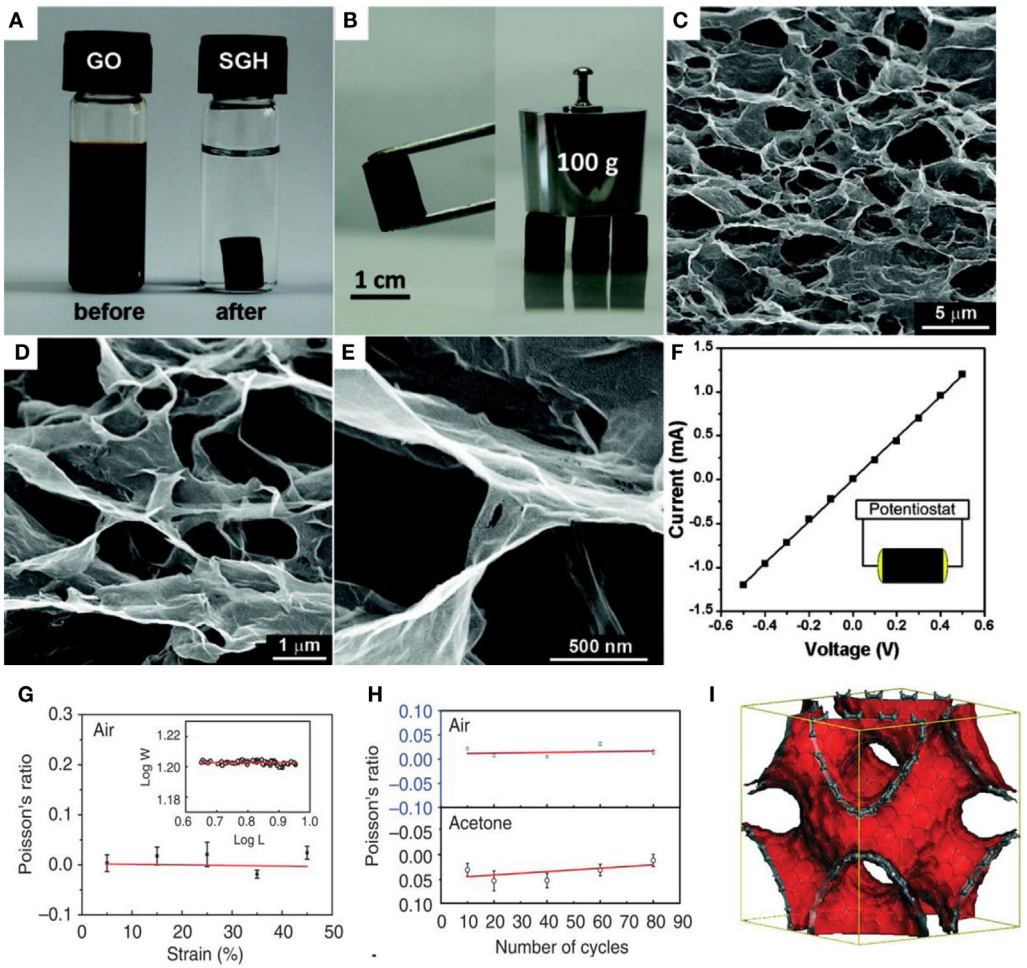

FIGURE 1 | **(A)** Photographs of a 2 mg/mL GO dispersion and after hydrothermal reaction at 180°C for 12 h, **(B)** photographs of a strong rGO hydrogel able to support weight, **(C–E)** SEM images of the GAs with various magnifications, **(F)** room temperature I–V curve of the GAs, inset shows the two-probe method, reproduced from Xu et al. (2010), with permission from American Chemical Society, **(G)** Poisson's ratio in air as a function of applied strain in the axial direction. **(H)** Poisson's ratio as a function of number of compression and release cycles along the axial direction. The blue and black colors are Poisson's ratios when the sponge is in air and in acetone, respectively. **(I)** The Schwartzite model for sp^2-carbon phases used for the Poisson's ratio modeling, reproduced from Wu et al. (2015a,b), with permission from Macmillan Publishers Limited.

showed high compressibility, and light weight, and was used for crude oil absorption.

Recently, Wu et al. (2015a,b) reported the self-assembly of graphene sheets into additive-free, uniform graphene-sponge with a synergistic arrangement of cork and rubber-like properties. They applied modified solvothermal reaction of GO colloidal dispersion in ethanol and consequent thermal annealing to form a material with super-elastic features such as rubber and near zero Poisson's ratio in all directions, similar to cork. These sponges possessed very low densities, repeatable compression, and complete recovery over a wide temperature in air (~900°C) and liquid (in liquid nitrogen ~196°C) without substantial degradation. Interestingly, this graphene sponge also exhibited high storage and loss moduli, which are independent of temperature and frequency. **Figures 1G–I** displays the Poisson's ratios of graphene sponge as a function of applied strain, number of cycles, and the Schwartzite model for sp^2-carbon phases utilized for the Poisson's ratio modeling.

Tang et al. (2010) reported noble-metal nanocrystal-induced graphene hydrogel made by employing hydrothermal reaction of GO suspension with noble-metal salt and glucose. They observed high catalytic activity and selectivity in the Heck reaction of their prepared Pd-induced graphene hydrogel. In addition, self-assembled graphene hydrogel can also be formed by hydrothermal treatment in the presence of divalent metal ions (Ca^{2+}, Co^{2+}, or Ni^{2+}) for *in situ* decoration of nanoparticles on 3D-Gs including metallic particles (Jiang et al., 2010) and alloys (Tang et al., 2015). The metal ion-induced self-assembly process was also employed for the formation of graphene-based aerogels, using α-FeOOH nanorods and magnetic Fe_3O_4 nanoparticles (Cong et al., 2012). Ren et al. (2013) developed a cost-effective technique for the fabrication of 3D freestanding

nickel nanoparticle/GA using self-assembling graphene with nickel nanoparticles during a hydrothermal process. Wu et al. (2012a,b,c,d) reported 3D nitrogen-doped GA-supported Fe_3O_4 nanoparticles made by hydrothermal self-assembly. This was followed by freeze drying and thermal treatment using polypyrrole as the nitrogen precursor. **Figures 2A–E** shows the fabrication process for 3D nitrogen-doped GA-supported Fe_3O_4 nanoparticles. The corresponding FESEM image revealed macroporous framework of graphene sheets with homogeneous dispersion of Fe_3O_4 nanoparticles. Xiao et al. (2013) established a facile and green method for the scalable synthesis of Fe_2O_3 particles decorated GA by hydrothermal method without additional reductant. Decorated 3D GAs were developed by self-assembly of graphene with simultaneous decoration with Fe_3O_4 nanoparticles using a modified hydrothermal reduction process (Xu et al., 2015a,b). Interestingly, metal oxide also used for the generation of mesopores on graphene nanosheets to develop 3D hierarchical porous GA fabricated by a hydrothermal self-assembly process. This was followed by *in situ* carbothermal reaction, as illustrated in **Figure 2F** (Ren et al., 2015).

Cross-Linking Agent-Induced Self-Assembly

Using organic amine and GO as precursors at mild temperature, Chen et al. (2013a,b) prepared nitrogen-doped graphene hydrogel using a hydrothermal method. The organic amine not only acts as the cross-linker to adjust the microscopic structure of 3D-Gs but is also used as the nitrogen precursor to form nitrogen-doped graphene hydrogel. Ultralight, highly compressible GAs have also been prepared by Hu et al. (2013) using the weak reducing and crosslinking agent ethylene diamine. They used a strategy of functionalization–lyophilization–microwave treatment to develop ultralight-compressible GA.

Ultra-light, compressible, fire-resistant GA was also prepared by Li et al. (2014) *via* simultaneous reduction and self-assembly of graphene oxide using ethylenediamine, followed by freeze-drying. Recently, Moon et al. (2015) designed highly elastic and conductive N-doped monolithic GA using hexamethylenetetramine as a reducer, nitrogen source, and graphene dispersion stabilizer *via* a combined hydrothermal and thermal annealing method (**Figure 3A**). An FESEM image (**Figure 3B**) revealed continuous cross-linking of the open-pore walls in N-doped GAs by an interconnected porous network between rGO layers in each cell wall. Conductivity was about 11.74 S m^{-1} at zero strain, and about 704.23 S m^{-1} under compressive strain of 80%. This is the largest electrical conductivity reported so far for 3D-GAs (**Figure 3C**). Ammonia was also used as the nitrogen precursor for the formation of N-doped GAs using hydrothermal treatment with GO solutions (Sui et al., 2015a,b,c). The product showed high surface area (830 m^2 g^{-1}), high nitrogen content (8.4 atom%), as well as good electrical conductivity and wettability.

Super-hydrophobic and super-oleophilic GA was fabricated by facile chemical reduction of GO solution using L-phenyl alanine (Xu et al., 2015a,b). This GA is hydrophobic, super-oleophilic, ultra-light weight exhibiting high surface area, remarkable absorption capacity and recyclability of oils and organic solvents and high mechanical properties.

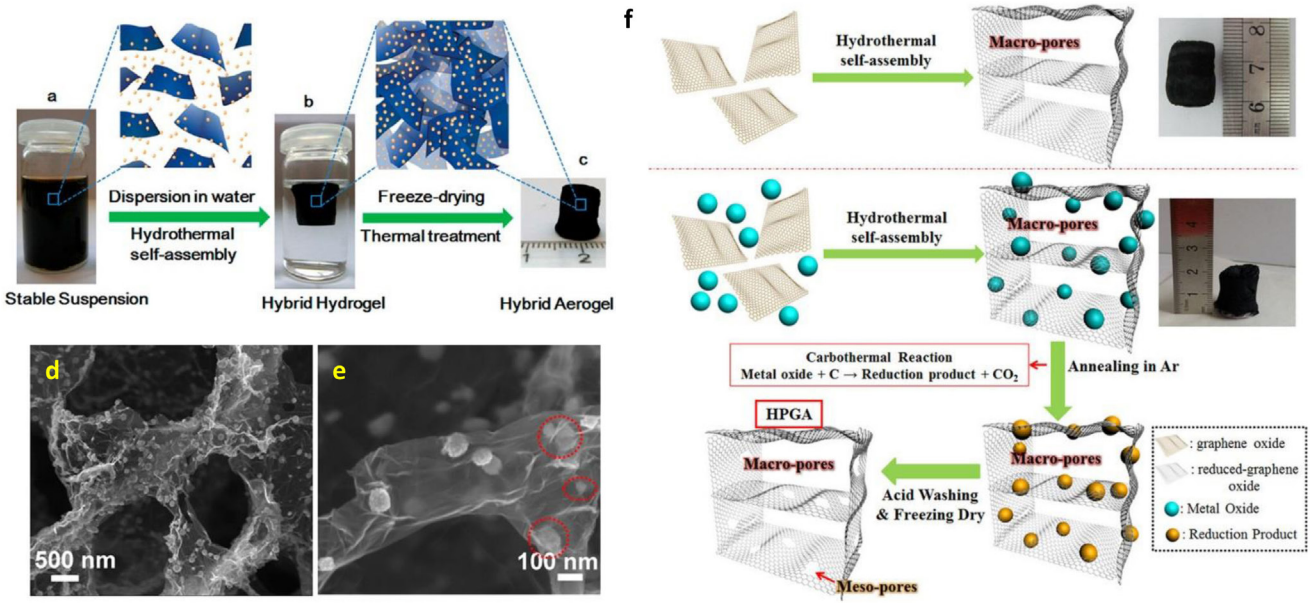

FIGURE 2 | **(A)** Fabrication process for the 3D Fe_3O_4/N-GAs catalyst: stable suspension of GO, iron ions, and PPy dispersed in a vial, **(B)** Fe- and PPy-supporting graphene hybrid hydrogel prepared by hydrothermal self-assembly and floating on water in a vial, and its ideal assembled model, **(C)** monolithic Fe_3O_4/N-GAs hybrid aerogel obtained after freeze-drying and thermal treatment, **(D,E)** typical SEM images of Fe_3O_4/N-GAs revealing the 3D macroporous structure and uniform distribution of Fe_3O_4 NPs in the GAs, reproduced from Wu et al. (2012a,b,c,d) with permission from American Chemical Society, **(F)** schematic diagram of the morphological formation of highly porous GAs, reproduced from Ren et al. (2015) with permission from Macmillan Publishers Limited.

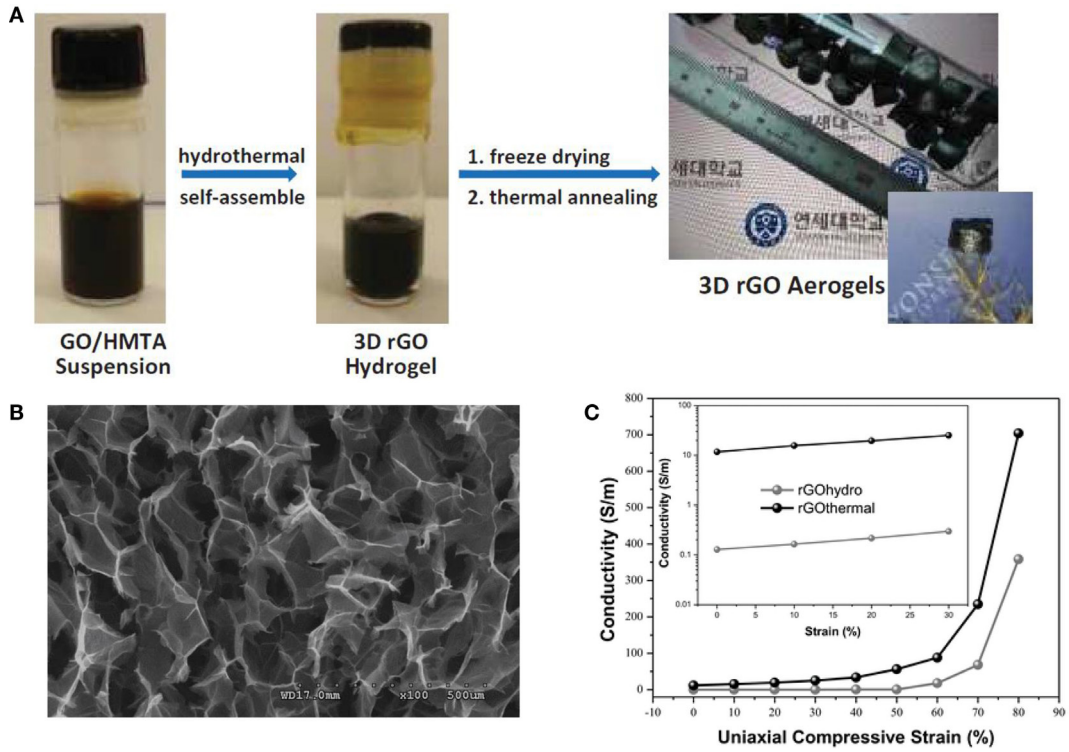

FIGURE 3 | (**A**) Photographs of the synthesis procedure for ultralight N-doped rGO thermal aerogels, **(B)** low-magnification SEM image of rGO thermal aerogels, **(C)** electrical conductivity of both rGO aerogels under compression via axial direction, reproduced from Moon et al. (2015) with permission from Wiley VCH.

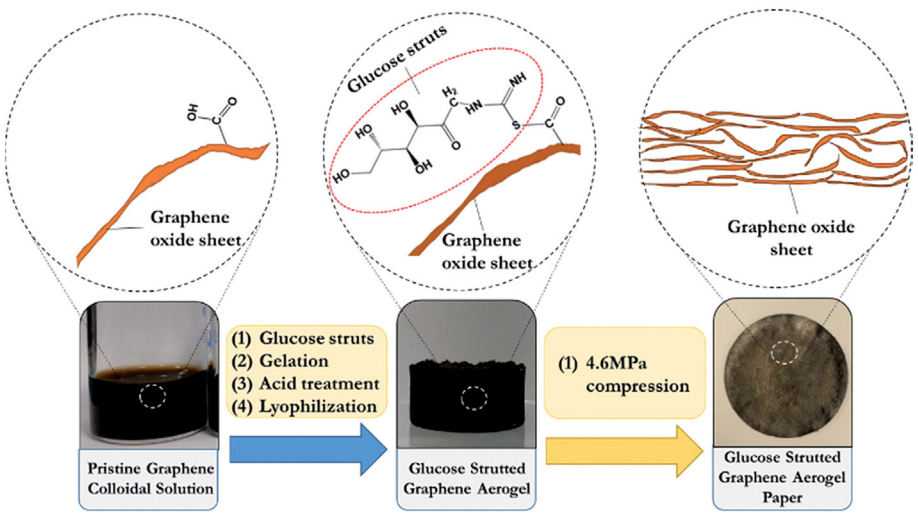

FIGURE 4 | **Schematic presentation of the synthesis proccedure for the glucose strutted graphene aerogel paper**. Reproduced from Lee et al. (2015), with permission from Royal Society of Chemistry.

Besides organic amine, layered double hydroxide (LDH) was also used as cross-linking for the self-assembly of GO to form GAs. Here, LDHs used as cross-linker to join GO nanosheets into a 3D framework through hydrogen bonds and cation–π interactions (Fang and Chen, 2014). These GAs demonstrated excellent hydrophilicity and structural stability in water, which assured the accessibility of their effective active sites in aqueous solution and overcomes the employment restrictions of neat GO aerogels due to their fragile morphology. Chen et al. (2013a,b) used a series of cross-linking agents containing –SH, $–NH_2$, –COOH, and –OH

groups for an examination of their reduction and self-assembly for GO dispersion. However, mercaptoacetic acid and mercaptoethanol were shown to form 3D-GAs. Actually, –SH groups reacted with hydroxyl or epoxy groups of GO to form covalent bonds resulting in the assembly of GO sheets *via* H-bonds. Recently, Lee et al. (2015) reported porous, flexible, free standing graphene-aerogel paper synthesized from acid-treated glucose-strutted GAs *via* mechanical compression (**Figure 4**). Sulfur groups in the glucose struts strengthen the GA papers owing to hydrogen bonding and thiol-carboxylic acid esterification. The hybrid aerogels exhibited high tensile strength (0.6 MPa), three times higher than GA paper without glucose struts.

Reducing Agent-Assisted Self-Assembly

Apart from organic amine, other reducing agents were also employed for the fabrication of 3D-G. Electrically conductive, mechanically strong GA was prepared using L-ascorbic acid (Zhang et al., 2011). The authors mentioned that compared to other reducing agents (hydrazine, $NaBH_4$, $LiAlH_4$), L-ascorbic acid did not generate any fumy by-products, the absence of which was serious for the formation of uniform gel. Other reducing agents such as $NaHSO_3$, Na_2S, ammonia boron trifluoride, vitamin C, hydroquinone, and sodium ascorbate have also been used to form 3D-GAs (Chen and Yan, 2011; Wu et al., 2012a,b,c,d). Three-dimensional assemblies of graphene have also been prepared using a novel, low-cost, environmentally friendly reducing medium combining oxalic acid and sodium iodide. It exhibited low density, highly porous structure, and electrical conductivity (Zhang et al., 2012). Yang et al. (2015) developed a facile, environmentally friendly, mild method to form GAs by thermal evaporation of GO suspension with $NaHCO_3$. This is an *in situ* reduction-assembly approach to form GAs. Reduced graphene oxide aerogel was also synthesized using simultaneous self-assembly and a reduction process with hypophosphorous acid and I_2 as reductant (Si et al., 2013). It exhibited large surface area of 830 $m^2\ g^{-1}$.

Polymer-Assisted Self-Assembly

Hong et al. (2015) established polymer-assisted self-assembly with a cross-linking approach for the development of reversibly compressible, highly elastic, durable GAs. Cross-linked rGO (x-rGO) was the factor responsible for providing high porosity along with large surface area owing to the re-stacking inhibition and steric hindrance of the polymer chains. They used two procedures for the formation of Gas, with and without crosslinking (**Figure 5A**). They used hypophosphorous acid and iodine as reducing agent for GO. They also utilized double cross-linking: initial cross-linking of GO with poly(vinyl alcohol) and second cross-linking with glutaraldehyde. A plausible cross-linking mechanism is indicated in **Figure 5B**. Importantly, the coupling of directional x-rGO networks with polymer viscoelasticity resulted in mechanical durability and structural bi-continuity,

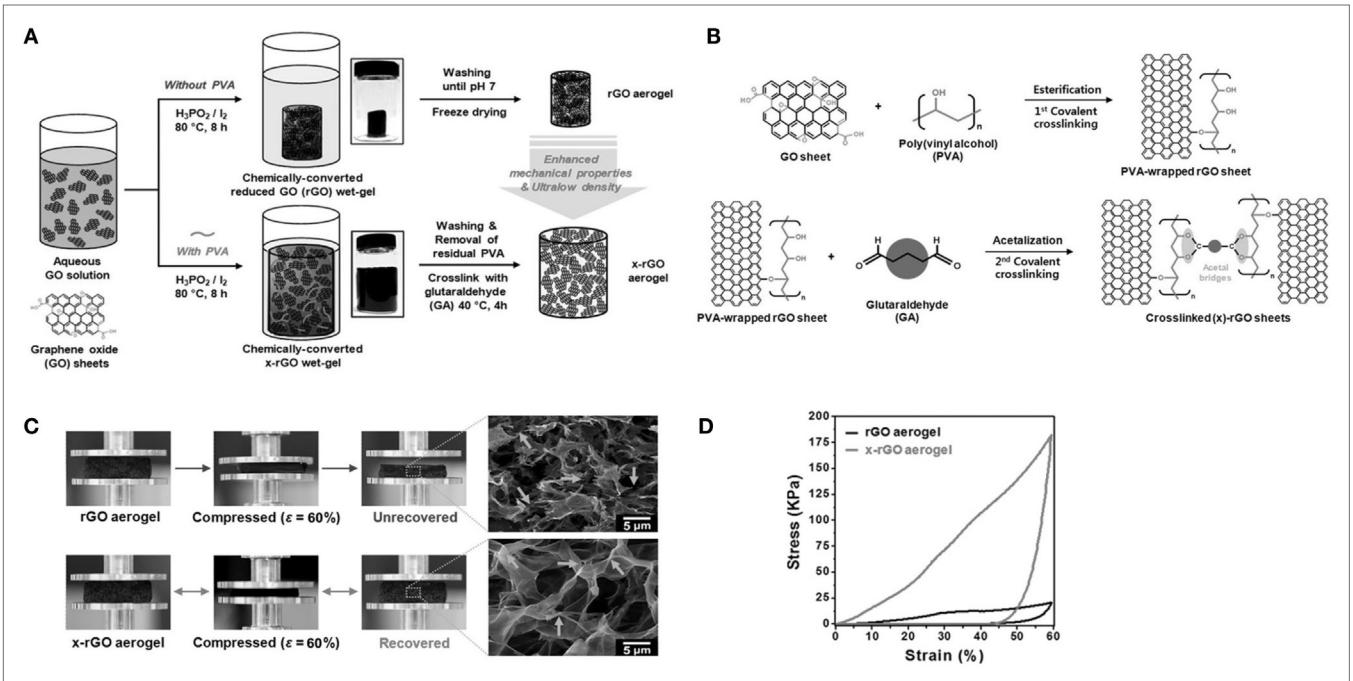

FIGURE 5 | **(A)** Schematic illustration of the different steps for fabricating both the rGO aerogel and x-rGO aerogel: Insets at center: digital photographs depict the as-prepared chemically converted rGO wet-gel (top) and x-rGO wet-gel (bottom) after the self-assembly process. These wet-gels were transformed to graphene-based aerogels by a freeze-drying method. **(B)** A plausible cross-linking mechanism between PVA-wrapped rGO sheets and GA. PVA-wrapped rGO sheets were covalently cross-linked by an acetal oxygen bridge. **(C)** Digital photographs and SEM images of rGO and x-rGO aerogels after compression with 60% strain. **(D)** Compressive stress–strain curves for rGO and x-rGO. Reproduced from Hong et al. (2015), with permission from Wiley VCH.

even under compressive strain (**Figure 5C**). Therefore, x-rGO aerogel exhibits higher compressive stress (8.6 times higher than rGO aerogel) as shown in **Figure 5D**.

A process for diffusion-driven self-assembly of GO nanosheets into various porous 3D macrostructures was designed by Zou and Kim (2014) *via* complexation of negatively charged GO sheets and positively charged, branched polyethyleneimine. Such diffusion of branched polyethylenimine molecules permits the complex to constantly propagate into foam-like networks with tailored porosity. Poly(*N*-isopropylacrylamide) (PNIPAM)-assisted GA was also synthesized to form mechanically robust, electrically conductive, and stimuli responsive super-elastic GAs (Qiu et al., 2014a,b). Here, graphene hydrogel was incorporated into the PNIPAM hydrogel to form a reinforced GA-based binary network hydrogel. Therefore, the construction of hierarchical nano filler networks in the polymer can offer an effective scheme for the development of high-performance polymer nanocomposites gel.

Sol–gel chemistry was used to design GA by the polymerization of resorcinol and formaldehyde in presence of sodium carbonate catalyst in GO solution (Worsley et al., 2010; Wang et al., 2013a,b,c; Zhu et al., 2015). Worsley et al. (2010) first utilized this sol–gel chemistry to cross link individual GO sheets to form GAs that exhibited high bulk electrical conductivity ($\sim 1 \times 10^2$ S/m), much higher than that of graphene assemblies by only physical cross-links ($\sim 5 \times 10^{-1}$ S/m). These GAs also have large surface area (584 m^2/g) and pore volume (2.96 cm^3/g) allowing these materials to be feasible candidates for catalysis, sensor, and energy storage applications. Highly N-doped porous GA was also obtained using the sol–gel chemistry of melamine–formaldehyde with GO solutions (Sui et al., 2015a,b,c).

Monomers of the corresponding polymers have also been used to synthesize cross-linked 3D-GAs by *in situ* polymerization, because the high molecular-weight polymers are insoluble or possess low hydrophilicity. Various polymers were prepared by this technique, in presence of GO solution, to form GAs. Pyrrole, aniline, and 4-ethylenedioxythiophene (EDOT) were used to form GAs with improved resiliency and electrochemical properties (Zhao et al., 2012a,b; Sun et al., 2014; Ye and Feng, 2014). Zhao et al. (2012a,b) proposed a unique strategy for the formation of polypyrrole–graphene foam by hydrothermal reaction of GO with pyrrole, followed by electrochemical polymerization of pyrrole. The PPy-G foam was shown to be robustly tolerant to high compressive strain without structural damage and loss of elasticity. Versatile, ultralight, N-doped GAs have been developed from hydrothermally treated aqueous suspensions of GO and pyrrole, followed by annealing under Ar gas (Zhao et al., 2012a,b). Apart from conducting polymers, other monomers including acrylamide and acrylic acid, were used to develop GAs.

Qin et al. (2015) reported a facile approach for transmuting fragile reduced graphene oxide (rGO) aerogel into super-flexible 3D architectures by incorporating water-soluble polyimide (PI), followed by freeze casting and thermal annealing. **Figure 6** shows compressive stress–strain curves with different set of strains, fatigue test at 50% strain for 2000 cycles, tensile stress–strain curves, and digital images of high level of deformations under bending and torsion. This rGO/PI aerogel nanocomposite exhibited low density, excellent flexibility, extraordinary reversible compressibility, good electrical conductivity, remarkable compression sensitivity, and excellent durability.

Li et al. (2016) first developed a cost-effective approach for the synthesis of robust GAs by employing *in situ* polymerization of acrylamide to strengthen graphene framework. This GA exhibited tough network structures, which restricted the capillary force of solvent evaporation during vacuum or air drying. This was the first time that GAs had been prepared without freeze drying; therefore, this represents an energy saving method with respect to freezing and supercritical drying processes. These GAs were further used to construct polymer/graphene composite foams by an infiltration-air-drying-crosslinking method. They prepared three different polymer/graphene composite foams, using cross-linked poly(dimethylsiloxane), cross-linked thermoplastic polyurethane, and cross-linked thermoplastic polyimide. Such shape-memory hybrid foams possessed very rapid retrievable shape-memory properties, compared to other reported shape-memory polymer foams. Importantly, the resulting ultralight cross-linked thermoplastic polyimide/graphene foams showed much enhanced thermotropic shape-memory performance (high compressibility, excellent fixing ratios, and high recovery ratios).

Influencing Factors for the Preparation of GAs from Gelation

From the previously mentioned overview, the concentration of GO, amount of additives, synthesis time, and temperature are the important factors affecting the fabrication of GAs, their structure, and their properties. Apart from these, pH, near infrared light, and drying method were also influential factors for preparation of GAs from gelation, because some of the stimuli induced controllable and reversible sol–gel processes of graphene and its derivatives. As stated earlier, there are two important drying methods for the fabrication of GAs: freeze drying and supercritical CO_2. Zhang et al. (2011) showed GAs obtained from supercritical CO_2 drying were darkish while freeze-dried GAs showed a more metallic luster. Importantly, GAs dried using the former technique support more weight, having larger surface area and pore volume, and higher electrical conductivity than those of freeze-dried GAs. Actually, the ice crystals formed during the freezing process are responsible for reducing the properties of GAs, although freezing temperature is also a significant parameter in controlling the porous structures and properties of GAs (Xie et al., 2013).

Self-assembled graphene hydrogel was obtained from reversible sol–gel transition upon exposure to different stimuli. Ruoff and his co-worker developed pH-mediated hydrothermal reduction to control the fabrication of compact high density GAs with different shapes (Bi et al., 2012). They reported that GAs obtained at pH 10 possessed plane surfaces, dense internal structures, good electrical conductivity, and good compressibility. Like the self-assembly from GO gelation, pH also contributed significantly to formation of GO/polymer composite hydrogel. For example, GO–PVA composites are highly pH sensitive because the pH value can tune the surface charge densities of the GO sheets as well as the electrostatic repulsion between them (Bai et al., 2010). Under basic (alkaline) conditions, the ionization of carboxyl groups on GO took place, leading to increased electrostatic repulsion among GO sheets.

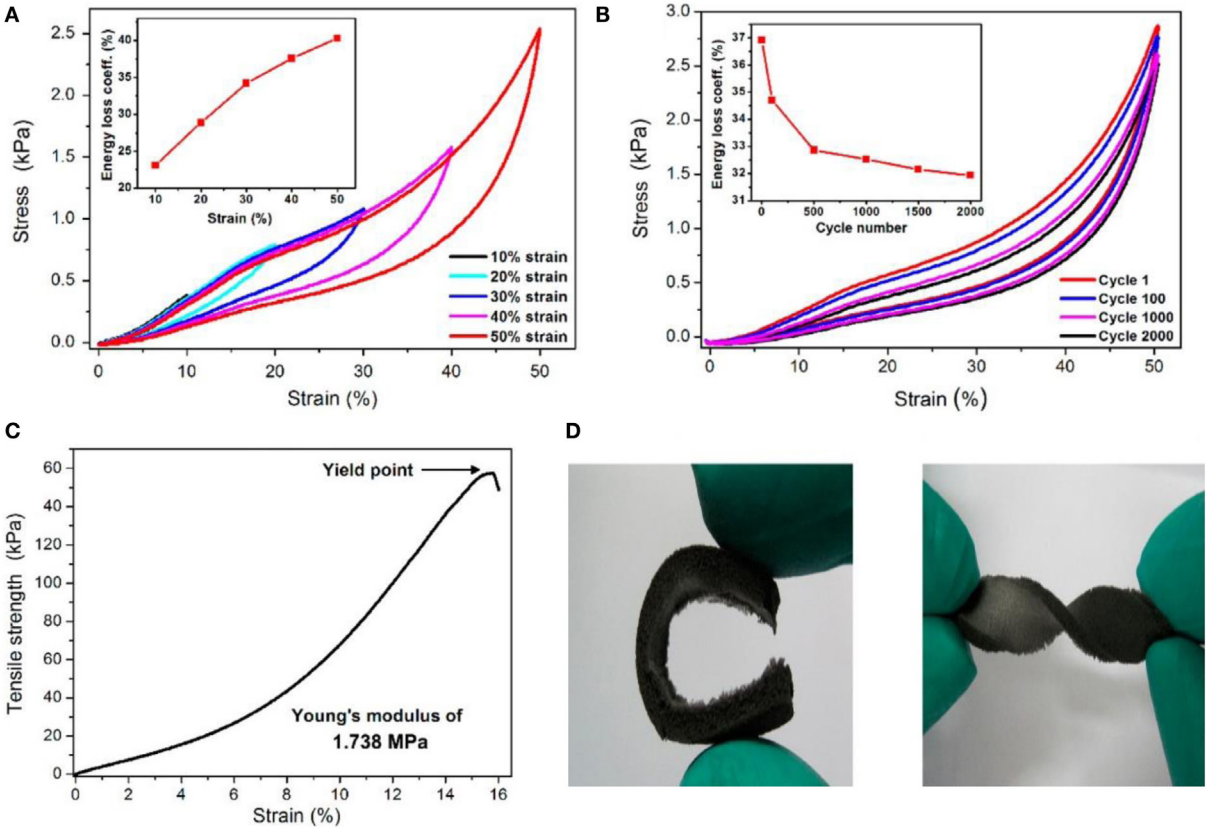

FIGURE 6 | **(A)** Stress–strain (σ–ε) curves of rGO/PI nanocomposite at different set strains: the inset indicates calculated energy loss coefficients of rGO/PI nanocomposite compressed under different strains. **(B)** Fatigue test of rGO/PI nanocomposite at 50% strain for 2000 cycles. Inset: energy loss coefficients over 2000 cycles. **(C)** Tensile σ–ε curve for the rGO/PI. **(D)** Digital images showing the high levels of deformation bend and torsion. Reproduced from Qin et al. (2015) with permission from the American Chemical Society.

From this, the hydrogel decomposed quickly owing to the lack of sufficient binding force. However, under neutral condition, all the functional groups on GO sheets can form strong H-bonds with the −OH rich PVA to form gel. The same findings were reported with GO/poly acrylic acid hydrogel – it formed gel more rapidly under a basic condition than when neutral (Liu et al., 2014).

Photothermal sensitivity is another important factor in formation of GO/polymer composite hydrogel (Lo et al., 2011; Wang et al., 2013a,b,c). The hydrogels showed a high degree of shrinkage under near-infrared laser irradiation, but after cooling, swelled back to the original form. The swelling/de-swelling transition of light-activated hydrogel is generally reversible and recyclable depending on exposure or non-exposure to lasers (Li et al., 2013). Wang et al. (2013a,b,c) took advantage of the thermoresponsive behavior of GO/polypeptide hydrogel to show tunable bending motions at specific positions.

Template-Directed Approach, Their Structures and Properties

As with self-assembly methods, template-directed methods have been promising techniques to produce GAs with more controlled and uniform morphologies and structures. Several template-directed methods have been described below.

Template-Directed CVD Approach

The template-assisted chemical vapor deposition (CVD) method is the most widely used method and provides far better structural integrity than in GAs formed by chemically derived graphene sheets. Chen et al. (2011a,b) first developed the nickel foam-directed CVD approach using CH_4 as the carbon source, at 1000°C under ambient pressure, for the formation of graphene film on Ni foam and subsequent etching of Ni using HCl solution. They also used a thin layer of poly(methyl methacrylate) on the graphene film surface before etching (to resist the collapse of the graphene network during etching), followed by removal of PMMA using hot acetone. The total procedure for the fabrication of GAs is shown in **Figure 7**. Other carbon sources like ethanol and acetylene were also utilized to grow graphene on Ni foam for the preparation of GAs (Cao et al., 2011; Yong et al., 2012). Generally, GAs prepared by the CVD method have high specific surface area (~850 $m^2\ g^{-1}$) compared to those prepared using chemical methods (~100–600 $m^2\ g^{-1}$) (Stoller et al., 2008; Bo et al., 2014).

Like Ni foam, Cu foam was also used as another template for the fabrication of CVD grown GAs (Kim et al., 2013). These materials showed outstanding electrical and mechanical properties with high flexibility and light weight. However, the

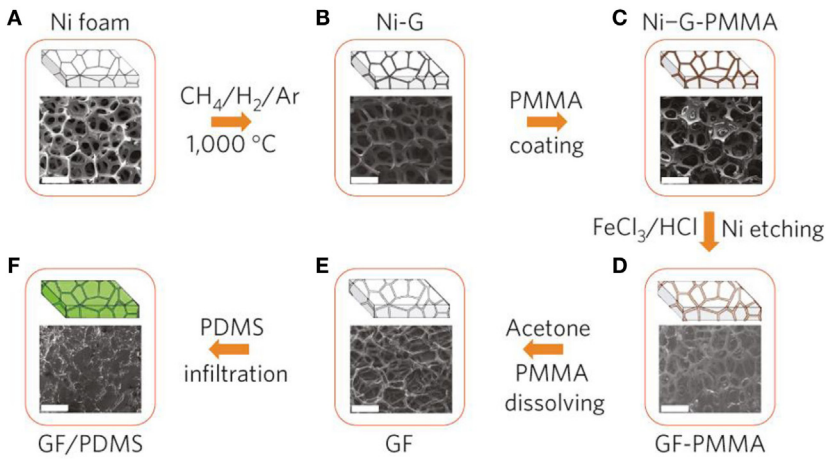

FIGURE 7 | Synthesis of a GF and integration with PDMS: CVD growth of graphene films (Ni–G), (A) as a 3D scaffold template and (B) using a nickel foam (Ni foam), (C) an as-grown graphene film after coating a thin PMMA supporting layer (Ni–G-PMMA), (D) a GF coated with PMMA (GF-PMMA) after etching the nickel foam with hot HCl (or $FeCl_3$/HCl) solution, (E) a free-standing GF after dissolving the PMMA layer with acetone, (F) a GF/PDMS composite after infiltration of PDMS into a GF. All the scale bars are 500 μm. Reproduced from Chen et al. (2011a,b) with permission from Macmillan Publishers Limited.

thermal diffusivity within such GAs was significantly less than that of single layer graphene (Lin et al., 2013). Three dimensional graphene foam was also prepared from Ni foam by Yavari et al. (2011) using a directed CVD approach. This product possessed ultra-high sensitivity for NH_3 and NO_2 sensing in air. Polyaniline was also employed to reunify with the template-directed CVD graphene foam to enhance the electrochemical properties of the hybrid foam (Dong et al., 2012).

Ice Template

Ice template-guided assembly has been used for fabricating GAs in aqueous solution (Vickery et al., 2009; Estevez et al., 2011). Importantly, unidirectional freezing is a well-known wet shaping technique for forming porous materials. Qiu et al. (2012) used the concept of the marriage of graphene chemistry with ice physics to develop ultralight, super-elastic, electrically conductive, graphene-based cellular monoliths. They developed cork-like hierarchical structure by freeze casting partially rGO, of which the structure was determined by the ice crystal template. Because ice crystal is anisotropic, rGO sheets are forced to align along the moving solidification front, yielding a highly ordered, layered assembly. The morphology and mechanism of the formation of super-elastic GA, along with compressive stress-strain curves and change to resistance upon 50% compression, are shown in **Figure 8**. Using the concept of directional freeze-drying of partially reduced graphene oxide (PrGO) aqueous suspension, several GAs have been prepared (He et al., 2013a,b; Xie et al., 2013).

Emulsion Template

It is a very complicated and critical procedure to develop GAs. This is because the size and structure of PrGO sheets essential to be prudently organized to adjust their interactions. Recently, Shi and his coworkers modified the hydrothermal method to form highly compressible GAs from an aqueous emulsion of GO with hexane droplets. GO sheets were accumulated surrounding hexane droplets as an emulsion template. As a result, these GAs exhibited excellent elasticity, low density, and good electrical conductivity. Menzel et al. (2015) also synthesized direct resistive heating of light-weight, compressible, thermally and electrically conductive, porous rGO aerogel *via* the emulsion-templating technique. They demonstrated Joule heating properties of an ultralight GA by repeated Joule heating up to 200°C, at comparatively low voltages (≈1 V) and electrical power inputs (≈2.5 W cm^{-3}). Because the power generation per unit volume is constant, the adjustable uniform temperature in GAs offered convenient, low voltage heating in a scalable way.

SiO_2 Template

The 3D printing template strategy is a unique strategy for the fabrication of 3D-GAs with designed macroscopic architectures (Zhu et al., 2015). GO ink was prepared using the concept of sol–gel chemistry of resorcinol–formaldehyde, ammonium carbonate as catalyst, and in the presence of fumed silica. Then the 3D printing method was used for the design of GA using GO ink followed by supercritical drying, annealing, and etching of fumed silica (**Figure 9**). Compressive stress–strain properties, energy loss coefficient and maximum stress variation with number of cycles, electrical resistance changes upon compression, and variation of Young's modulus with density of 3D-GAs, are presented in **Figure 9**. This method advanced the production of porosity tailored, mechanically robust, super compressible, high electrically conductive hierarchical 3D-GAs with large surface area.

Lithographical Template

Lithography is another novel approach to the design of GAs. This is a multistep process involving creation of 3D carbon by

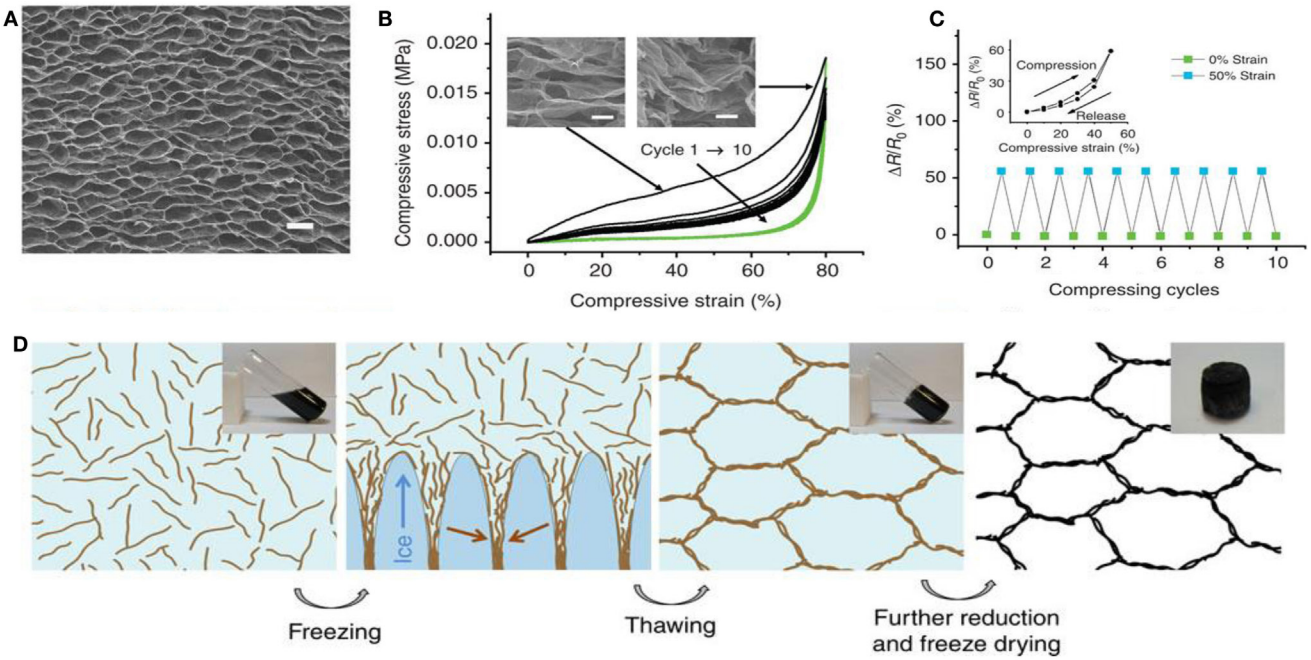

FIGURE 8 | **(A)** SEM top-view image of a graphene monolith, **(B)** compressive stress–strain curves upto10 cycles of loading (black lines) and unloading (green lines). The insets show the corresponding SEM images under compression at different strains. **(C)** Electrical resistance change upon compression up to 50% of strain for over 10 cycles. The inset shows the result for one cycle. **(D)** Schematic showing the formation mechanism of the cork-like monolith by freeze casting. Insets shows the photographs of the corresponding samples. Reproduced from Qiu et al. (2012) with permission from Macmillan Publishers Limited.

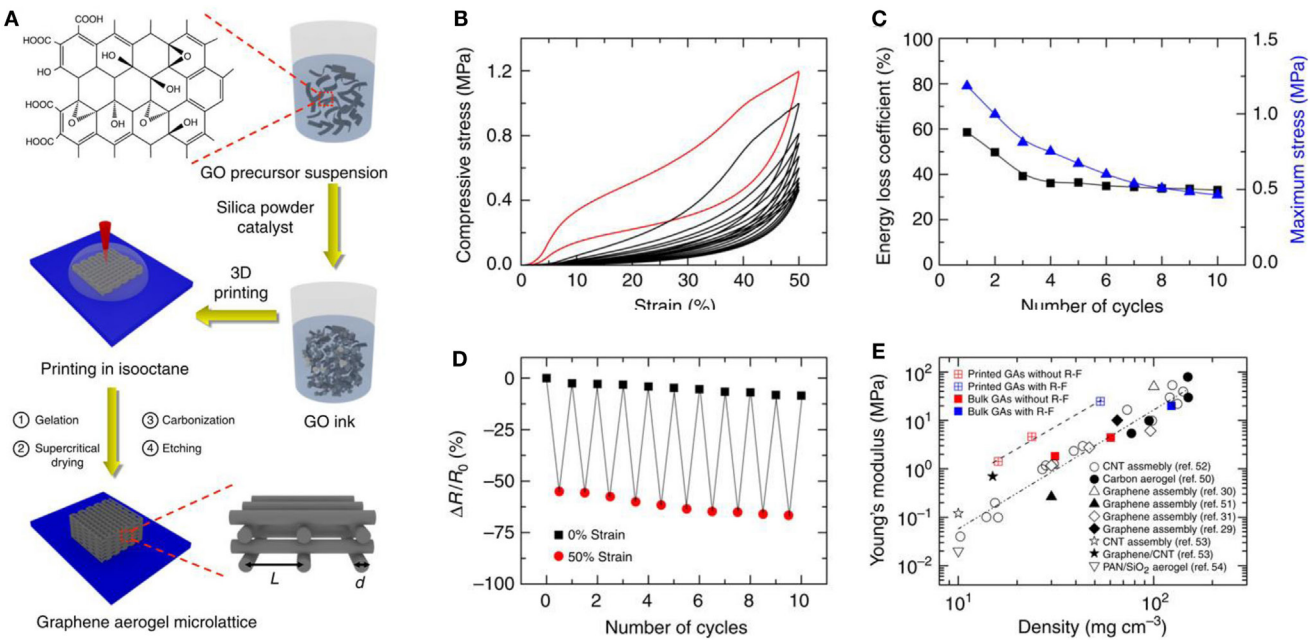

FIGURE 9 | **(A)** Schematic of the fabrication process of GAs using 3D printing template. The in-plane center-to-center rod spacing is defined as L, and the filament diameter is defined as *d*. **(B)** Compressive stress–strain curves of 10 cycles of loading/unloading. **(C)** Maximum stress and energy loss coefficient during 10 cycles. **(D)** Electrical resistance change when repeatedly compressed up to 50% of strain for 10 cycles. **(E)** The relationships of Young's modulus with density of bulk and printed graphene aerogels. Reproduced from Zhu et al. (2015) with permission from Macmillan Publishers Limited.

interface lithography, followed by sputtering of 3D amorphous carbon with Ni and subsequent annealing at 750°C to convert 3D graphitic monoliths and accomplish acidic etching (Xiao et al., 2012). Here, 3D pyrolyzed photoresist films were used for the conversion of 3D porous graphene. This is a unique technique to form 3D graphene foams utilizing a host *via* a lithographic patterning technique.

Other Novel Approaches

Jung et al. (2015) developed porous 3D GAs from graphene suspensions *via* an electrochemical exfoliation method. They controlled the porosity of the graphene network by adjusting the content of electrolyte during the exfoliation process. Maiti et al. (2014) synthesized GAs using interfacial gelation strategy with Zn foils. Because the reduction potential at pH 4 of reduced GO (rGO)/GO (−0.4 V^- SHE) is higher than that of Zn/Zn^{2+} (−0.76 V vs. SHE), rapid self-assembly of GO formed gel on Zn foil followed by etching the Zn foil using HCl solution, and subsequently freeze drying to form robust GAs. Wang et al. (2013a,b,c) used a polystyrene template for the preparation of GAs v*ia* calcination. These GAs exhibited large surface area and high electrical conductivity. Besides PS, PMMA was also used as the support for GO self-assembly followed by removal of PMMA using chloroform. These GAs also exhibited large surface area and porosity (Trung et al., 2014). Gao and his coworkers developed a template free, synergistic assembly of graphene sheets and CNT ribs for the scalable production of macroscopic, multiform (1D, 2D, and 3D), ultralight aerogels (Sun et al., 2013). The ideal combination of graphene and CNT offered exciting properties including ultralow density, outstanding temperature invariant elasticity, good electrical conductivity, and high thermal stability.

MULTIFUNCTIONAL APPLICATIONS OF GRAPHENE AEROGELS

Batteries

Rechargeable lithium-ion batteries (LIBs) have recently become widely used as power sources, particularly for electric/hybrid electric vehicles, portable electronics, and renewable energy systems (Chen et al., 2011a,b; Zhong et al., 2013). Therefore, to get high-performance Li-battery applications, the design of novel electrode materials plays an important role in Li storage performance. In this context, graphene is one of the most widely used anode materials in commercial Li-batteries (Xiao et al., 2013; Ren et al., 2015). To date, a variety of forms of graphene have been utilized as efficient anode materials in LIBs, including metal-oxide based 2D graphene materials, hetero-atom doped graphene materials, and GAs. Among these, GAs with 3D hierarchical structure are an emerging anode material for LIBs. These GAs facilitate multidimensional electron transportation passageways and reduced transportation spaces between electrode and electrolyte; thereby enhancing battery performance and cyclic stability. Sometimes, metal/metal oxide and metal sulfide were integrated in GAs to form hybrid materials for LIB cathodes (Zhou et al., 2014).

Graphene aerogel provides excellent support for metal oxides to enhance the overall Li-ion battery performance of the resulting hybrid materials. Chen et al. (2011a,b) prepared self-assembly GAs/Fe_3O_4 composites as anodes for LIB applications. This composite showed good rate performance – it exhibited high capacity (≈990 mA h g^{-1}) at current density of 800 mA g^{-1} and retained at ≈730 mA h g^{-1} even at 1600 mA g^{-1} current density. It retained 1100 mA h g^{-1} even after fifty charge-discharge cycles at different current densities, indicating good cyclic stability. Such promising electrochemical performance is owing to the robust interaction between Fe_3O_4 and the graphene sheets in the aerogel. This makes spacers, resulting in the adsorption of Li ions on both sides of graphene nanosheets, as well as insertion/de-insertion of Li ions during charging and discharging. Xiao et al. (2013) developed self-assembled Fe_2O_3/GAs as anode materials for Li-battery applications due to the synergistic interaction between uniformly dispersed Fe_2O_3 in GAs. This resulted in short diffusion path length for the transport of Li ions, as well as providing a highly conductive network. It displayed excellent reversible capacity of 995 mA h g^{-1} after 50 cycles at a charge/discharge rate of 100 mA g^{-1} and offered reversible capacity of 372 mA h g^{-1} at the high rate of 5000 mA g^{-1}. Pre-encapsulated Fe_3O_4 nanospheres were also used to crosslink 3D graphene foams for enhanced Li storage (Wei et al., 2013). They used a functionalized Fe_3O_4–GO hybrid for better interaction with other GO solutions to provide Fe_3O_4 crosslinked 3D graphene foam. They reported that the material possessed initial reversible capacity of 920.3 mA h g^{-1}, which is much higher than Fe_3O_4 and functionalized Fe_3O_4–GO hybrid, and indicates a high rate capability (**Figures 10A,B**). Cycling performance also showed the superiority of this graphene hybrid foam; for example, it showed reversible capacity of 1059 mA h g^{-1} after 150 cycles (**Figure 10C**). Some GAs/metal oxide composites also have shown to exhibit good Li-battery applications as illustrated in **Table 1**.

Rutile SnO_2 was also integrated *in situ*, in a controlled way, inside GAs. This is shown to exhibit enhanced Li-ion storage performance (1176 mA h g^{-1} for the 1st cycle and 872 mA h g^{-1} for the 50th cycle at 100 mA g^{-1}) with respect to its two counterparts, namely, rough nanoparticles@3D-GA and anisotropic SnO_2@2D graphene sheets (618 and 751 mAh/g for the 50th cycle at 100 mA/g, respectively) (Yao et al., 2015). **Figures 11A–C** displays galvanostatic cyclic measurements (for 1st, 2nd, and 50th cycles) at 100 mA/g current density, along with cycling and rate performances. The fact is that a 3D structure having large surface area and mesoporous structure remarkably improved conductivity by offering multidimensional channels for electron transport, as well as enhanced Li-ion diffusion in the electrolyte (**Figure 11D**). Apart from GAs, anisotropic SnO_2 assembled from nanorods with large surface area provided additional approaches for accessing Li ions. Wang et al. (2014) also synthesized solvothermal-induced SnO_2/N-doped GAs as anode materials for Li storage. Because of the hierarchical, porous nature along with its large surface area, the electrode showed high rate capability (614 mA h g^{-1} at 6000 mA g^{-1}) with good cycling stability (905 mA h g^{-1} after 1000 cycles at 2000 mA g^{-1}).

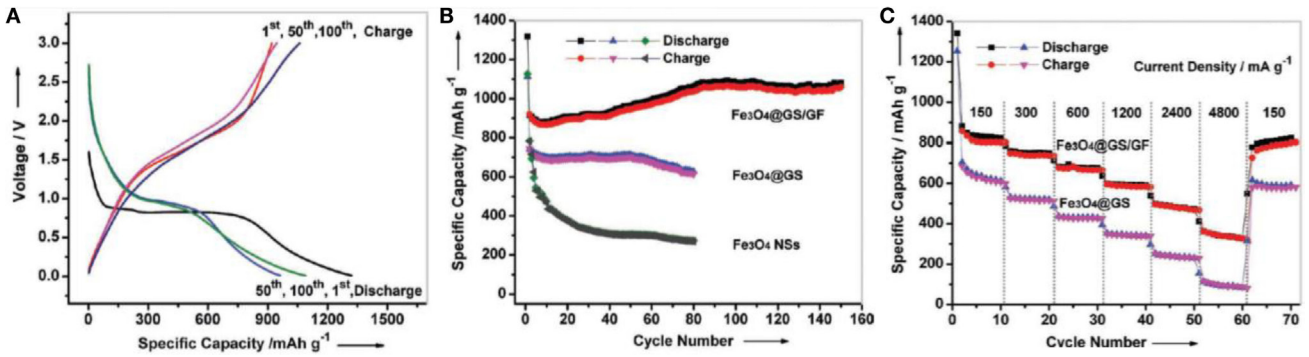

FIGURE 10 | **(A)** Galvanostatic charge/discharge profiles of Fe_3O_4 @GS/GF at a current density of 93 mA g^{-1}, **(B)** cycling performance of Fe_3O_4@GS/GF, Fe_3O_4@GS, and Fe_3O_4 NSs at a current density of 93 mA g^{-1}, **(C)** cycling performance of Fe_3O_4@GS/GF and Fe_3O_4@GS at various current densities. Reproduced from Wei et al. (2013) with permission from Wiley VCH.

TABLE 1 | Li-ion battery performance of graphene aerogel/metal oxide composites.

GAs/metal oxide composites	Method of preparation	Initial specific discharge capacity	No. of cycles and their corresponding capacity
GAs/Fe_3O_4 composites (Chen et al., 2011a,b)	Self-assemble process	≈2006 mA h g^{-1} at current density of 200 mA 1g^{-1}	Fifty cycles, 1100 mA h g^{-1}
GAs/Fe_2O_3 (Xiao et al., 2013)	Hydrothermal process	1515 mA h g^{-1} at current density of 100 mA g^{-1}	Fifty cycles, 995 mA h g^{-1}
Fe_3O_4 crosslinked 3D graphene foam (Wei et al., 2013)	Hydrothermal process	1320 mA h g^{-1} at current density of 93 mA g^{-1}	150 cycles, 1059 mA h g^{-1}
GAs/Co_3O_4 composites (Ren et al., 2015)	Hydrothermal process	2900 mA h g^{-1} at current density of 100 mA g^{-1}	88 cycles,1050 mA h g^{-1}
GA/Co_3O_4 composites (Garakani et al., 2014)	Hydrothermal process	1200 mA h g^{-1} at current density of 100 mA g^{-1}	200 cycles, 832 mA h g^{-1}
GAs/SnO_2 composites (Liang et al., 2013)	Self-assembly process at 90°C	2100 mA h g^{-1} at current density of 100 mA g^{-1}	100 cycles, 832 mA h g^{-1}
GAs/CoO composites (Dong et al., 2015)	Hydrothermal process	951 mA h g^{-1} at current density of 100 mA g^{-1}	100 cycles, 544 mA h g^{-1}
N-doped GAs/SnO_2 Composites (Tan et al., 2014)	Hydrothermal process	1963 mA h g^{-1} at 200 mA g^{-1}	100 cycles, 1100 mA h g^{-1}
N-doped GAs/SnO_2 Composites (Wang et al., 2014)	Solvothermal process	2000 mAh g^{-1} at 500 mAg^{-1}	200 cycles, 1200 mA h g^{-1}
GA/TiO_2 composite (Qiu et al., 2014a,b)	Hydrothermal process	956.2 mA h g^{-1} at 100 mAg^{-1}	50 cycles, 200 mA h g^{-1}

Recently, mesoporous TiO_2 nanocrystals have also been grown *in situ* on GAs for LIBs (Qiu et al., 2014a,b). A TiO_2/GA hybrid electrode, in the presence of glucose, showed good cycling stability compared to that without glucose. Remarkably, even when 67 wt% of the ingredients was active, it showed reversible capacity of 99 mA h g^{-1}: four times higher than that of pristine TiO_2 nanocrystals. Actually, in the absence of glucose, TiO_2/GA showed poor dispersion of TiO_2 nanocrystals, which hindered transfer of electrons and storage of Li ions.

Wang et al. (2015a,b) used nanostructured $LiFePO_4$ wrapped, N-doped GA as cathode material for high-power LIBs. Such unique structure provided pathways for rapid electron transfer and ion transport and short Li ion diffusion length in $LiFePO_4$ crystals. As a result, this form of hybrid aerogel exhibited high rate capability (78 mA h g^{-1}) and long cycling stability (89% retention of capacity over 1000 cycles at 10 current rate). MnO_2-anchored N-doped GAs were also found to exhibit promise as anodes for LIB (Sui et al., 2015a,b,c). They showed very high discharge capacity (909 mA h g^{-1}) after 200 cycles at 400 mA g^{-1} current density, compared to individual MnO_2 or N-doped GAs. Such hybrid aerogels also possessed good rate capability and cyclic stability due to the synergistic contribution of uniformly dispersed MnO_2, and the large surface area and porosity of the N-doped GAs.

Recently, research on 3D porous graphene-based materials for Li-S batteries has grown fast owing to superior features like large surface area, and porosity that can anchor large amounts of sulfur and lithium polysulfide (Jiang et al., 2015; Xie et al., 2015). Therefore, apart from the applications of GAs in LIBs, GAs have shown amazing improvement in reversible capacity, rate capability, and cyclic stability; as cathodes for Li-S batteries. Xie et al. (2015) used B-doped GAs loaded with sulfur as cathode materials for Li-S batteries. The authors suggested that, with respect to N-doped and undoped GAs, sulfur embedded, B-doped GAs delivered higher capacity (994 mA h g^{-1}) at 0.2°C after 100 cycles, with good rate capability.

Supercapacitors

Supercapacitors involve two types of energy storage mechanism: electrical double layer capacitors (EDLC) and pseudo-capacitors (Jiang et al., 2013). Both are surface phenomena that occur during the charge/discharge process so the behavior of supercapacitors is highly dependent on the surface area of materials. In this regard, graphene, with large surface area (~2630 m^2 g^{-1}) with high conductivity (~2000 S cm^{-1}) is an ideal medium for enhancing the capacitance of both EDLCs and pseudo-capacitors (Zhai et al., 2011; Bello et al., 2013). Recently, GA, with large pore size, pore volume, and surface area have been applied as unique support

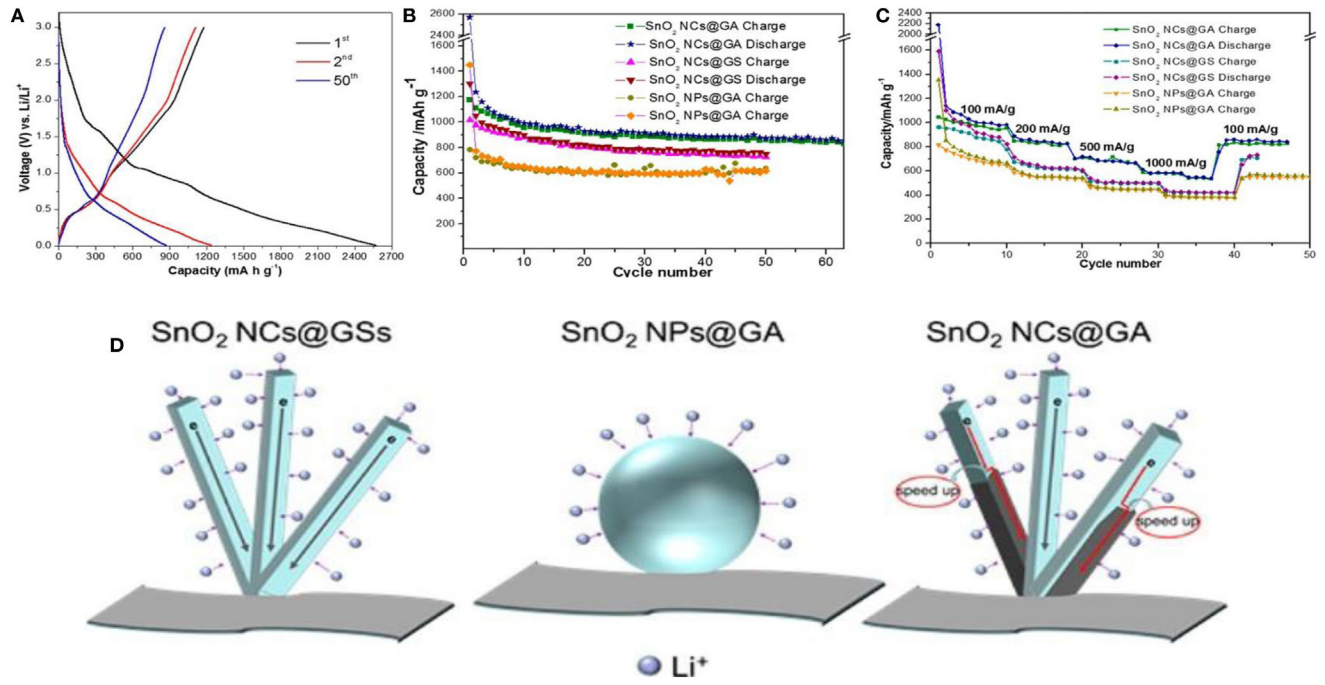

FIGURE 11 | **(A)** Galvanostatic discharge/charge profiles of SnO_2 NCs@GA for the 1st, 2nd, and 50th cycles at a current density of 100 mA/g. **(B)** Cycling performance of SnO_2 NCs@GA, SnO_2 NPs@GA, and SnO_2 NCs@GS at a current density of 100 mA/g. **(C)** Rate performance of SnO_2 NCs@GA, SnO_2 NPs@GA, and SnO_2 NCs@GS at different current densities. **(D)** Schematic comparison of SnO_2 NCs@GS, SnO_2 NPs@GA, and SnO_2 NCs@GA in terms of lithium access and electron transport. Compared with sphere-shaped nanoparticles, the NCs consisting of 1D nanorods, provide additional active sites for lithium access, attributed to their increased electrode–electrolyte contact area. SnO_2 NCs grown on graphene sheets (SnO_2 NCs@GS) suffer from severe self-stacking, which results in shrinking of the surface area. The graphene wrapping in SnO_2 NCs@GA can also accelerate electron transport by providing more shortcuts to the graphene highway. Reproduced from Yao et al. (2015) with permission from the American Chemical Society.

for supercapacitor applications due to the maximum exposure of their surfaces to electrolyte. Apart from these, the combination of 3D interconnection structure and excellent electron conductivity of graphene, has made GAs promising materials for use as electrodes in supercapacitors. Wang et al. (2014) prepared GA by sol–gel chemistry using resorcinol–formaldehyde followed by electrochemical deposition of manganese oxide on GAs for outstanding supercapacitor electrode materials. Jung et al. (2015) developed porous GAs via electrochemical exfoliation and reported it to be a promising electrode for supercapacitor applications. **Figure 12** displays the CV curves, galvanostatic charge–discharge curves, and calculated specific capacitance at different current densities, with different freezing temperature along with Ragone plots of GAs. Therefore, it can be observed that these GAs not only showed a specific capacitance of 325 F g^{-1} at 1 A g^{-1} and an energy density of 45 W h kg^{-1} without the sacrifice of power density in 0.5M H_2SO_4 aqueous electrolyte, but also exhibited high electrochemical stability and electrode uniformity. Supercapacitor performances of some GA-based electrodes are explained in **Table 2**.

Although we know graphene paper acts as a promising flexible electrode, restacking and degradation issues limit the use of graphene paper as a flexible electrode. Recently, Lee et al. (2015) synthesized flexible, free standing, glucose-strutted graphene-aerogel paper as a promising electrode for supercapacitor applications. It showed specific capacitance of 311 F g^{-1} at current density of 1 A g^{-1} and showed high specific capacitance (262 Fg^{-1}) even at 20 A g^{-1} current density. Hong et al. (2015) developed a double cross-linking strategy for the formation of reversibly compressible, highly elastic, durable GAs using PVA and glutaraldehyde for energy storage devices under limiting conditions. The cross-linked rGO aerogels retain >140% and >1400% enhancements in the gravimetric and volumetric capacitances, respectively, at 90% compressive strain while both volumetric and gravimetric capacitances of rGO were not measured at the breaking point (~60% compressive strain). Therefore, cross-linked GAs displayed stability of the volumetric capacitance under both static and dynamic compression. Such enhancement of gravimetric and volumetric capacitance is due to dense, porous, compact bi-continuous morphology *via* the effective delocalization of PVA cross-linked networks through electrically conductive rGO sheets. Volumetric capacitance of the cross-linked aerogel under sequentially repeated compression and relaxation for 1000 cycles indicated the volumetric capacitance while under compression slightly decreased after 500 cycles, while the volumetric capacitance under the relaxation state was almost constant. The cycle performance test after 2000 charge/discharge cycles of cross-linked GAs, indicated promising cyclic stability.

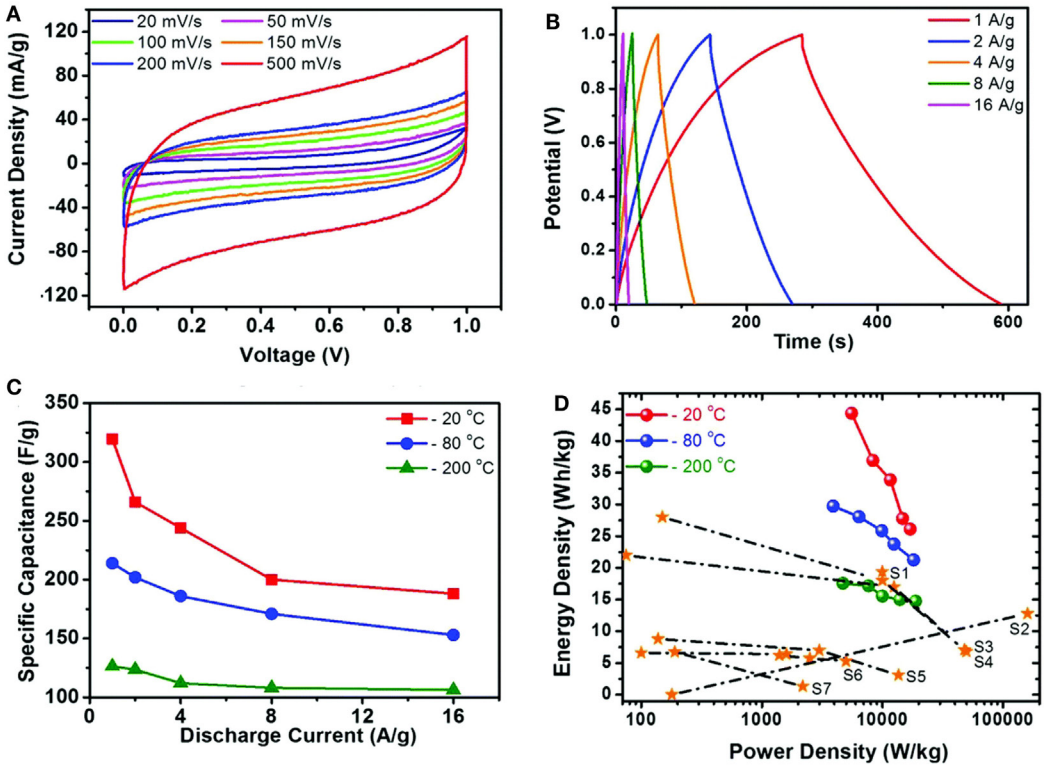

FIGURE 12 | **(A)** The CV curves of the graphene aerogel supercapacitors at various scan rates. **(B)** Galvanostatic charge/discharge curves of the graphene aerogel at different current densities. **(C)** Specific capacitances at different freezing temperatures, calculated from CV curves **(D)** Ragone plot of the samples in this work compared to those of previous reports. Reproduced from Jung et al. (2015) with permission from the Royal Society of Chemistry.

Introducing "stabilizer" or "spacer" into GAs is one of the most promising ways to enhance the supercapacitor performance, especially in using pseudo-active materials, such as metals (Li et al., 2011), metal oxides (Yu et al., 2011; Zhu et al., 2011; He et al., 2013a,b), conductive polymers (Huang et al., 2012; Tai et al., 2012; Gao et al., 2013; Ye et al., 2013), and carbon nanotubes (Zhu et al., 2012). Ye et al. (2013) developed 3D hierarchical graphene/polypyrrole nanotube hybrid aerogels for supercapacitor applications. Deformation tolerant devices are much needed for high-tech electronics of irregular forms. Zhao et al. (2012b) developed highly compressible graphene–polypyrrole hybrid foam as an efficient electrode for high-compression tolerant supercapacitors. For this purpose, they used a two-electrode capacitor with controlled compression state (**Figure 13A**). It exhibits specific capacitance of 350 F g^{-1} at 1.5 A g^{-1}. **Figure 13B,C** displays the CV curves as well as galvanostatic charge–discharge curves under 0 and 50% compression, and their cyclic stability. The foam electrode showed remarkable compression tolerance without varying the specific capacitance, even up to 1000 cycles, suggesting excellent electrochemical stability of the foam electrode (**Figure 13D**). Polyaniline was also used by Yang et al. (2014) for the preparation of graphene/polyaniline hybrid aerogel for promising supercapacitors.

The capacitive performance of GAs can be further enhanced by chemical doping of hetero atoms in GAs or by etching. In either case, the presence of electro-active species and larger surface area of pores play important roles for achieving higher specific capacitance of the GAs. A versatile, ultralight N-doped GA using pyrrole as the nitrogen precursor displayed specific capacitance of 484 F g^{-1} at 1 A g^{-1} current density and high cyclic stability even after 1000 cycles (Zhao et al., 2012a,b). Yu et al. (2015a,b) prepared sulfur-doped GAs using thioglycolic acid as the sulfur precursor with hypophosphorous acid and iodine. These GAs were shown to exhibit high specific capacitance of 445 F g^{-1} at a scan rate of 5 mV s^{-1} with good rate capability (78.2%) and 73.4% cyclic stability even after 1500 cycles. These results were due to the pseudocapacitive nature of S, and to the large surface area of GAs that facilitates fast ion diffusion in the electrolyte. Sui et al. (2015a,b,c) prepared N-doped GA from ammonia and GO, to explore supercapacitor behavior. These GAs were found to exhibit high specific capacitance of 223 F g^{-1} at 0.2 A g^{-1} with good cyclic stability.

Interfacial gelation was used to create 3D, custom-shape engineered rGO on Zn foil for use in high-rate capable supercapacitor electrodes (Maiti et al., 2014). The product retained 97.8% of its initial capacity even after 4000 cycles at a fast rate of 10 mA cm^{-2}. It also demonstrated high energy density of 2.73 μW h cm^{-2} and high areal power of 369.8 mW cm^{-2}. They mentioned that such high values of GAs were attributed to the high electrical conductivity and fluent ion transport behavior. Actually, the

TABLE 2 | Capacitive performance of various graphene aerogel based electrodes.

GAs based electrode	Rate capability	Specific capacitance (at scan rate or current density)	Cyclic stability	Energy density (at current density or power density)
MnO_2/GAs (Wang et al., 2014)	85% (from 25 mV s^{-1} to 1000 mV s^{-1})	410 F g^{-1} at 2 mV s^{-1} at high MnO_2 loading of 61 wt%	95% after 50,000 cycles at 1000 mV s^{-1}	–
GAs from graphene suspension using electrochemical exfoliation (Jung et al., 2015)	–	325 F g^{-1} at 1 A g^{-1}	98% coulombic efficiency of the initial capacitance after 5000 cycles	45 W h kg^{-1} at 1 A g^{-1}
GAs-Ni foam hybrid (Ye et al., 2013)	49% (from 2 to 20 A g^{-1})	366 F g^{-1} at 2 A g^{-1}	60% after 2000 cycles at 10 A g^{-1}	-
Glucose-strutted GAs paper (Lee et al., 2015)	84% (from 1 to 20 A g^{-1})	311 F g^{-1} at 1 A g^{-1}	92% after 4000 cycles at 20 A g^{-1}	–
GAs using L-ascorbic acid (Zhang et al., 2011)	60% (from 50 mA g^{-1} to 20 A g^{-1})	128 F g^{-1} at 50 mA g^{-1}	–	–
GAs by a self-assembly approach (Wu et al., 2012a,b,c,d)	71% (from 100 mA g^{-1} to 2000 mA g^{-1})	153 F g^{-1} at 100 mA g^{-1}	–	21.1 W h kg^{-1} at 100 mA g^{-1}
Hypophosphorous acid and iodine reduced GAs (Si et al., 2013)	63% in 1M H_2SO_4 and 74% in 6M KOH (from 0.2 to 20 A g^{-1})	278.6 F g^{-1} in 1M H_2SO_4 and 211.8 F g^{-1} in 6 M KOH at 0.2 A g^{-1}	98.5% in 1 M H_2SO_4 and 85% in 6M KOH	9 W h kg^{-1} at power density of 100 W kg^{-1}
H_3PO_4 activated GAs (Sun et al., 2015)	69% (from 0.2 to 30 A g^{-1})	204 F g^{-1} at 0.2 A g^{-1}	92% after 10,000 cycles at 5 A g^{-1}	7.4 W h kg^{-1} at power density of 100 W kg^{-1}
3D Hierarchical graphene/ polypyrrole nanotube hybrid (Ye et al., 2013)	55% (from 0.5 to 10 A g^{-1})	253 F g^{-1} at 0.5 A g^{-1}	95% after 2000 cycles at 10 A g^{-1}	–
Self-assembled Graphene/PANI hybrid aerogels (Yang et al., 2014)	64% (from 0.25 to 2 A g^{-1})	520.3 F g^{-1} at 0.25 A g^{-1}	89% after 500 cycles at 1 A g^{-1}	–
Graphene/polypyrrole aerogel (Sun et al., 2014)	76% (from 0.5 to 1 A g^{-1})	304 F g^{-1} at 0.5 A g^{-1}	58.26% after 50 cycles at 1 A g^{-1}	–

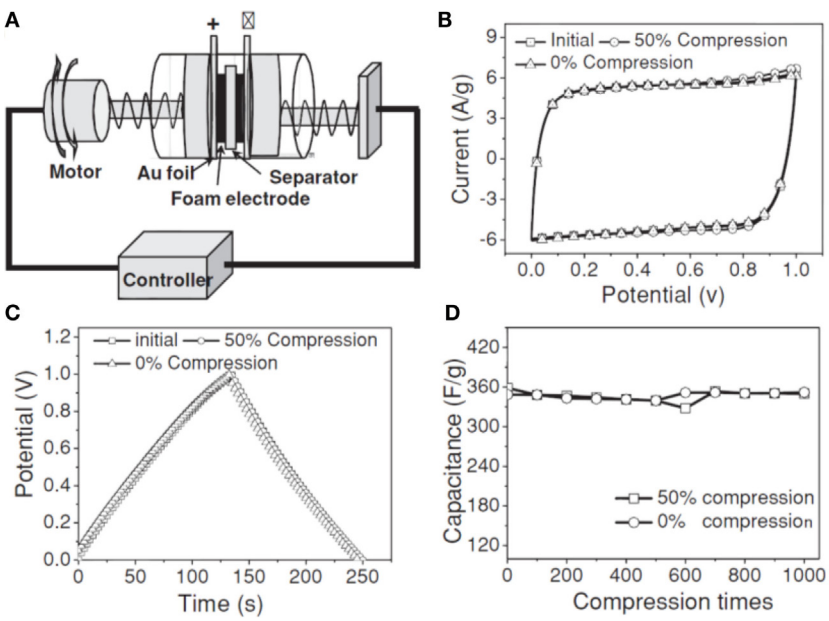

FIGURE 13 | **(A)** Schematic drawing of PPy-G based supercapacitor devices. **(B)** CVs at 30 mV/s of the compressible PPy-G foam electrodes under 0 and 50% compression for one cycle. **(C)** The corresponding galvanostatic charge-discharge curves at a current density of 1.5 A g^{-1}. **(D)** The specific capacitances at different compressions for 1000 cycles. Reproduced from Zhao et al. (2012b) with permission from Wiley VCH.

electrically conductive, quasi-parallel interconnected graphene network surrounding open pores not only offered high rate capability but also provided large areal capacity simultaneously.

Metal-nanoparticle decorated GAs also appear to be promising electrode materials for asymmetric supercapacitors. Yu et al. (2015a,b) synthesized functionalized GAs decorated with Pd nanoparticles as efficient asymmetric supercapacitor anode materials. This GA composite showed high specific capacitance (175.8 F g^{-1} at 5 mV S^{-1}), remarkable retention of rate capability (48.3% retention even after 10-fold increase of the scan rate), and good reversibility, owing to its large surface area and high electrical conductivity. Mesoporous silica has also been integrated with 3D interconnected macroporous GAs (Wu et al., 2012a,b,c,d) to generate high specific surface area with hierarchical porous features. Benefiting from the synergistic combination of meso and macroporous structures, GAs revealed high specific capacitance (226 F g^{-1}), high rate capability, and excellent cyclic stability. Wu et al. (2015a,b) synthesized self-assembled V_2O_5/GA that showed high specific capacitance (486 F g^{-1}), high energy density (68 W h kg^{-1}), and good cyclic stability due to their hierarchical porous structure. Hybrid GA of MnO_2/$MnCO_3$/rGO has been used directly as an electrode for asymmetric supercapacitors without adding polymer binders or conductive adhesives (Liu et al., 2015a,b,c). Interestingly this asymmetric supercapacitor exhibited an energy density of 17.8 W h kg^{-1} with a power density of 400 W kg^{-1}.

Graphene foam was also prepared using a Ni-foam-templated ethanol-CVD method (Cao et al., 2011). The authors suggested that this graphene foam acted as a good platform for metal oxide decoration for supercapacitor applications. Therefore, such GAs produced using the template-directed CVD method were shown to provide good electrochemical properties, and were recognized as favorable candidates for supercapacitors. For example, NiO/GAs composites were shown to exhibit specific capacitance of 816 F g^{-1} at 5 mV s^{-1} with good rate capability.

Ju et al. (2014) designed graphene/porous carbon aerogel *via* a simple green technique for high-performance, flexible, solid state supercapacitors. These materials showed specific capacitance of 187 F g^{-1} at 1 A g^{-1} and retained a high specific capacitance (140 F g^{-1}) even at 10 A g^{-1}. This was due to their large surface facilitating the transport and diffusion of ions and electrons through the porous structure of the aerogel. Polyethyleneimine-modified graphene oxide was also used for the preparation of graphene with carbon aerogel, by using sol–gel polymerization of resorcinol–formaldehyde (Lee et al., 2013). This aerogel displayed high specific capacitance of 205 F g^{-1} and low equivalent series resistance (0.55 Ω). Chen et al. synthesized a new hybrid aerogel of graphene quantum dots/GAs which showed specific capacitance of 268 F g^{-1}, almost 90% higher than that of pristine GAs (136 F g^{-1}) (Chen et al., 2014). This aerogel was evaluated to be useful for symmetrical supercapacitor electrodes.

Sensors

Three-dimensional GAs offer ideal platforms for various electrochemical sensing, bio-sensing, and strain sensing purposes owing to the unique properties, including their large active surface area. Such GAs, decorated with metal or metal oxide/hydroxide nanostructures, could provide high energy density and electrochemical stability (Yan et al., 2015).

Recently, Qin et al. (2015) reported a flexible graphene/polyimide nanocomposite foam, which shows remarkable compression sensitivity and excellent, persistent stability for use in strain sensors. They studied the pressure responsive properties of rGO/PI monoliths and electronic resistance-variation ratios with respect to strain (**Figure 14**). The pressure responsive behavior showed a low-pressure regime from 0 to 1.5 kPa exhibiting increased slope with a sensitivity of 0.18 kPa^{-1}. In the large-pressure regime (3.5–6.5 kPa), the sensitivity of the rGO/PI composite was 0.023 kPa^{-1} owing to variation of tunneling of charges carried between adjacent rGO sheets in the monoliths. Moreover, under a wide range of compressive strains during loading and unloading, this monolith showed variation of electronic resistance synchronization with applied strains. The variation of change in resistance with time maintained a plateau until the release of stress. It showed also good cycling stability – even after 2000 loading/unloading cycles. The variation of electronic resistance displayed reasonably excellent repeatability, with no decrease of resistance of the composites. Measurements during the bending cycles exhibited stability, and the resistance variations were consistent, indicating extraordinary electromechanical stability of the rGO/PI nanocomposite.

Table 3 reports sensor performance of few Gas-based composites. Lv et al. (2016) prepared super-elastic graphene/carbon nanotube aerogels by integrating CNTs into 3D graphene and investigated them for use in a strain-gage sensor with a tunable strain/pressure sensing capability. The sensitivity of the strain-gage of graphene/CNTs aerogels could be tuned by controlling the aerogel density. In compressive strain tests, the gage factor of the proposed sensor reached 230 and 125%, at strain of 30 and 60%, respectively.

Wu et al. (2015a,b) established a 3D-bonded spongy graphene material with density similar to that of air. These graphene sponges exhibited both rubber and cork-like features. They displayed Poisson's ratios in both the axial and radial directions that were near-zero, and were largely strain-independent during reversible compression. Freestanding, mechanically stable, highly electrically conductive graphene foam has been prepared using a two-step process that includes dip-coating and pyrolysis. The foam showed ultralow density of ≈1.2 mg cm^{-3}, elastic modulus of 90 ± 29 kPa, and compressive strength of 4.7 ± 1.6 kPa, corresponding to a porosity of more than ≈99.8%. The graphene foam-PDMS composites could be used for a range of low and high-strain/pressure sensors owing to the differences in sensitivity provided by different densities of GF (Samad et al., 2015).

A graphene foam with a hierarchical structure can be further enhanced using a directional freezing technique and afterward high thermal treatment for a large-scale strain-gage sensor (Kuang et al., 2013). The foam showed admirable compression recovery over a wide range of strain, and good electrical conductivity of up to 0.5 S cm^{-1}, with exceptional piezoresistive capabilities.

Yavari et al. (2011) developed a macroscopic 3D graphene foam network for high sensitivity gas sensing. Such sensors demonstrated parts-per-million level detection of NH_3 and NO_2 in air at room-temperature and atmospheric pressure. Importantly,

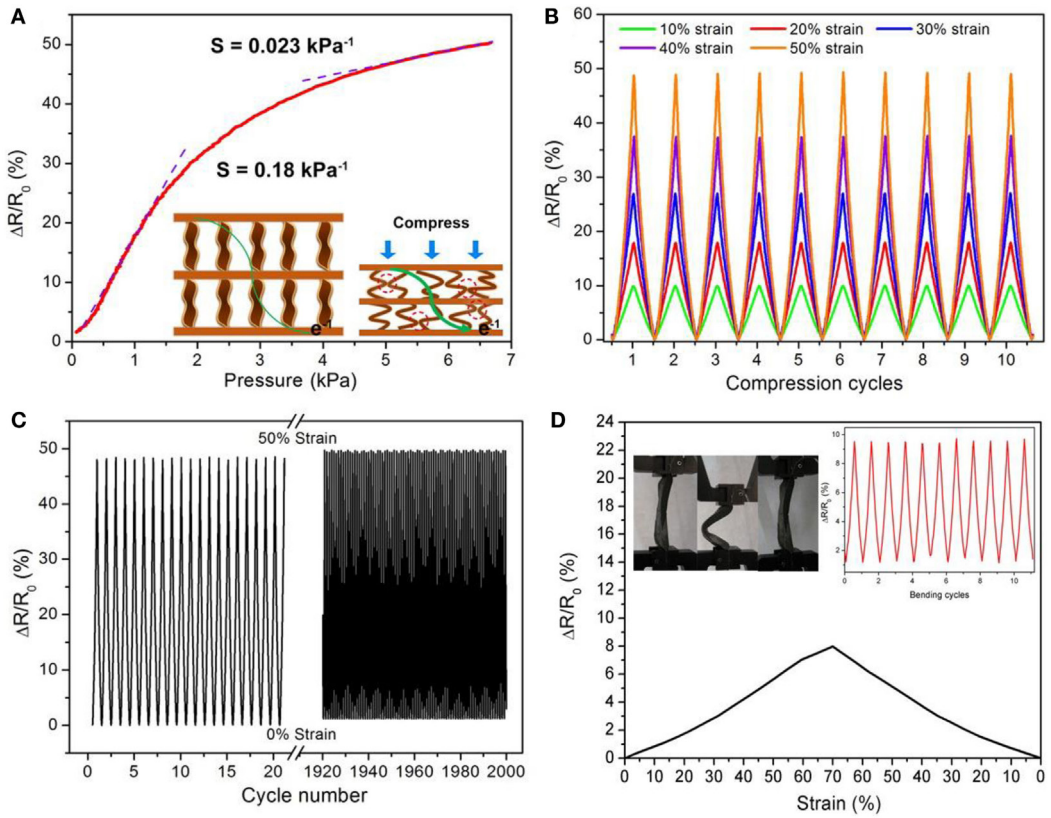

FIGURE 14 | **(A)** Pressure–response curves for rGO/PI nanocomposite. Inset: current changes in responses to compression and release. **(B)** Multiple-cycle tests of change in resistance with different applied strains. **(C)** Cycling stability test of rGO/PI composite under repeated applied strain of 50% for 2000 cycles. **(D)** The variation of resistance with strains of the rGO/PI nanocomposite in a typical bending cycle. The strain refers to ΔL/L0 = (L0 LP)/L0, where L0 and LP denote the distance between two ends of the nanocomposite with and without applied pressure, respectively. Inset: electrical-resistance change of rGO/PI nanocomposite under mechanical deformation from bending and then straightening for each cycle. Photographs of the bending process. Reproduced from Qin et al. (2015) with permission from the American Chemical Society.

the graphene foam structures showed high sensitivity of gas detection in the parts-per-million range because of charge carrier transport through the mechanically robust, but flexible, macroscale graphene foam network.

Because of high electron transfer rate, porous structure and their chemical and biological inertness GAs exhibit ultrasensitive chemical response. Juanjuan et al. (2014) developed nitrogen-doped activated GA/gold nano particles for electrochemical detection of hydroquinone (HQ) and *o*-dihydroxy benzene (DHB). The detection limit is 1.5×10^{-8}M for HQ and 3.3×10^{-9}M for DHB. This method provides the advantage of sensitivity, repeatability, and stability compared with other HQ and DHB sensors. GAs-gold nanostar hybrid has also been used by Hongxia et al. (2015) for the electrochemical detection of HQ and DHB with ultrahigh sensitivity and selectivity. Wang et al. (2015a,b) also developed glucose oxidase sensor based on GAs/gold nanoparticle hybrid materials. This biosensor was found to exhibit remarkable sensitivity (257.60 μA mM^{-1} cm^{-2}), an approximate linear detection range of glucose concentration (50–450 μmol L^{-1}), and a detection limit of 0.597 μmol L^{-1}. Oxalic acid senor was also developed by GAs (Liu et al., 2015a,b,c). The sensor showed a linear relation toward OA detection in the concentration of 4–100 μM with a low detection limit of 0.8 μM. Cao et al. (2013) developed GAs as templates for construction of graphene-based composites, which are further used as electrochemical sensors. The detection limit of H_2O_2 was found as low as 8.6 nM by using the composite consisting of 3DGNs, MWCNTs and Pt nanoparticles.

Actuators

Recently, soft actuators have been intensively researched as promising candidates for use in soft robotics, flexible displays, and haptic devices. Though GAs are eminently suitable materials for soft actuators due to their super-lightness, high compressibility, stretchability, and porosity, few papers related to GA-based actuators have been published, until recently.

Xu et al. (2015a,b) succeeded in synthesizing Fe_3O_4 nanoparticle-decorated 3D-GAs by self-assembly of graphene and nanoparticles using hydrothermal reduction, as shown in **Figure 15**. The incorporation of Fe_3O_4 nanoparticles in the aerogels makes the aerogels respond to magnetic stimuli. This aerogel shows great magnetic field-induced actuations of 52 and 35% along the radial and axial directions, respectively. Graphene

TABLE 3 | Sensory performance of graphene aerogel based composites.

GA-based composites	Sensor type	Sensing element	Sensitivity
Graphene/polyimide nanocomposite foams (Qin et al., 2015)	Strain sensor	–	0.18 kPa^{-1} at a low-pressure regime from 0–1.5 kPa
Graphene/carbon nanotube aerogels (Lv et al., 2016)	Strain-gage sensor	–	Gage factor of the proposed sensor reached 230% at a strain of 30%
Graphene/iron oxide aerogel (Xu et al., 2015a,b)	Magnetic field-induced strain	–	52% Reversible magnetic field-induced strain
3D periodic graphene aerogel microlattices (Zhu et al., 2015)	Pressure sensor	–	Energy loss coefficient decreased from 60 to 30% in the first three cycles, and then remained constant
3D Graphene foam network (Yavari et al., 2011)	Gas sensor	NH_3 and NO_2	30% resistance change at room temperature at lower NH_3 concentration,1000 ppm and 60% resistance change at NO_2 concentration of 200 ppm
N-doped GAs/gold nano particles (Juanjuan et al., 2014)	Electrochemical sensor	Hydroquinone (HQ) and *o*-dihydroxy benzene (DHB)	1.5×10^{-8}M for HQ and 3.3×10^{-9}M for DHB
GAs-gold nanostar hybrid (Hongxia et al., 2015)	Electrochemical sensor	HQ and DHB	4.3×10^{-10}M for HQ and 2.1×10^{-10}M for DHB
GAs/gold nanoparticle hybrid (Wang et al., 2015a,b)	Biosensor	Glucose oxidase	0.597 μmol L^{-1} for glucose oxidase
GAs (Liu et al., 2015a,b,c)	Biosensor	Oxalic acid	0.8 μM for oxalic acid
GAs/MWCNTs/Pt nanoparticles composites (Cao et al., 2013)	Electrochemical sensor	H_2O_2	8.6 nM for H_2O_2

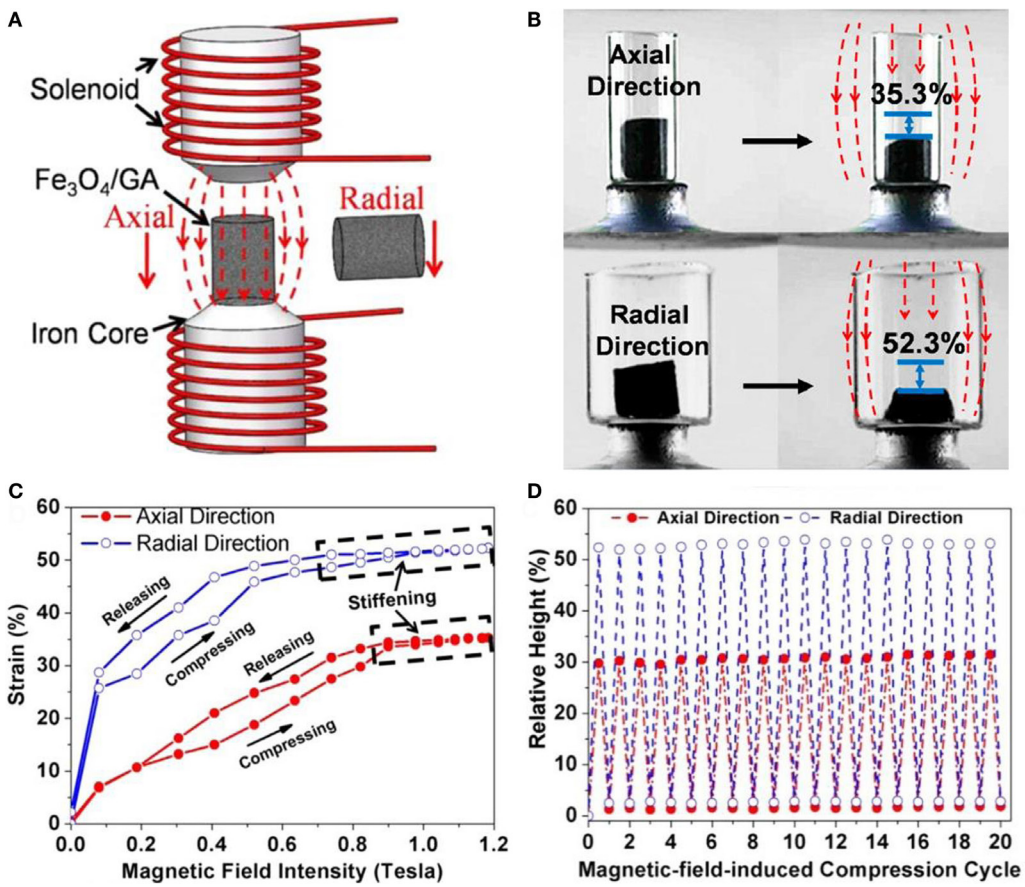

FIGURE 15 | **(A)** Schematic diagram of the experimental setup for actuation tests and **(B)** magnetic induced compression along the axial and radial directions of Fe_3O_4/GA. **(C)** Actuation strains as a function of the magnetic field intensity and **(D)** height changes for 20 cycles. Reproduced from Xu et al. (2015a,b) with permission from the American Chemical Society.

TABLE 4 | The actuation performances of graphene aerogel based actuators.

Gas-based actuators	Actuation type	Actuation performance	Durability
GAs/Fe_3O_4 composites (Xu et al., 2015a,b)	Magneto-responsive actuation	Strain of 52% (radial)/35% (axial) @ 1.2 T	No change after 20 cycles
Graphene-CNT aerogel/ epoxy composites (Liu et al., 2015a,b,c)	Shape memory actuation	Bending angle of 81° @60 V	–
GAs/trans-1,4-polyisoprene composite (Li et al., 2016)	Shape memory actuation	Strain of 80% @10 V	99% after 10 cycles

and carbon nanotube compound, aerogel-based shape-memory composites, exhibiting actuation performance under a voltage of 60 V, were developed by Liu et al. (2015a,b,c). Epoxy, known as a shape-memory polymer, was used for the shape recovery of the composites. In addition, ultralight x-TPI/graphene foams have been studied for high-performance shape-memory actuations with a high thermotropic property. This results in low actuation-voltage (6–10 V) and in short recovery time (8 s) (Li et al., 2016). Specifically, the foams recover their original shape with a recovery ratio of 99% for 10 cycles. Actuation performance of few GAs are described in **Table 4**.

CONCLUSION AND PROSPECTS

Flourishing nanotechnology and incredible innovation regarding GAs have opened up major potential for their wider application in energy storage devices (batteries and supercapacitors), sensors, and actuators. Importantly, GAs can be easily integrated into devices. Moreover, they are superior to 2D graphene-based materials due to a long list of uniquely beneficial characteristics (e.g., very high surface area, high electrical and thermal conductivity, high chemical and electrochemical stability, high elasticity and flexibility, high hydrophobicity). Therefore, they can be demonstrated to provide a facile strategy by which to bridging the gap between the nanoscale properties of graphene and practical macro-scale applications. To facilitate the challenges faced in the design of these progressive materials, this article presents a broad review about the most current evolution in detailed synthesis procedures, properties, fundamental understanding, and their wide applications as electrode materials in batteries, supercapacitors, sensors, and actuators. GAs are not only designed by assembly of graphene nanosheets for practical applications but might also be used as support materials on which to load inorganic nanoparticles and various organic or polymeric molecules. Such loading can be used to improve GA functionalities or overcome the restrictions of pure GAs for specific target applications, by combining the merits of all their components.

Although, a lot of effort has been devoted to these emerging materials, there are still many challenges to address in developing real world applications. First, the efforts to address the non-homogeneity of GAs with respect to porosity, pore size, and functional groups; lack the controlled fabrication methods and deep knowledge of the assembly mechanism. Second, it is crucial to develop facile methods for creating high-quality GAs fit for real, specific applications. Third, precise characterizations are required to understand the surface chemistry of GAs. Fourth, the fabrication of high-quality materials and their applications in actuators are still in the primary stage. Although there are several challenges to be met in the near future, it is expected that GAs will become one of the most promising materials in the world, by providing new opportunities for revolutionary changes in science and technology, and most importantly, in real life.

AUTHOR CONTRIBUTIONS

Dr. MK wrote the synthesis part of review article, and JK and JO wrote the application part of the graphene aerogels. Prof. I-KO decided to write the review article regarding graphene aerogels, outlined the whole contents and carefully wrote the review article.

FUNDING

This work was partially supported by Creative Research Initiative Program (2015R1A3A2028975) funded by National Research Foundation of Korea (NRF).

REFERENCES

Bai, H., Li, C., Wang, X., and Shi, G. (2010). A pH-sensitive graphene oxide composite hydrogel. *Chem. Commun.* 46, 2376–2378. doi:10.1039/C000051E

Bello, A., Fashedemi, O. O., Lekitima, J. N., Fabiane, M., Dodoo-arhin, D., Ozoemena, K. I., et al. (2013). High-performance symmetric electrochemical capacitor based on graphene foam and nanostructured manganese oxide. *AIP Adv.* 3, 082118. doi:10.1063/1.4819270

Bi, H., Yin, K., Xie, X., Zhou, Y., Wan, N., Xu, F., et al. (2012). Low temperature casting of graphene with high compressive strength. *Adv. Mater.* 24, 5124–5129. doi:10.1002/adma.201201519

Bo, Z., Shuai, X., Mao, S., Yang, H., Qian, J., Chen, J., et al. (2014). Green preparation of reduced graphene oxide for sensing and energy storage applications. *Sci. Rep.* 4, 4684. doi:10.1038/srep04684

Cao, X., Shi, Y., Shi, W., Lu, G., Huang, X., Yan, Q., et al. (2011). Preparation of novel 3D graphene networks for supercapacitor applications. *Small* 7, 3163–3168. doi:10.1002/smll.201100990

Cao, X., Zeng, Z., Shi, W., Yep, P., Yan, Q., and Zhang, H. (2013). Three-dimensional graphene network composites for detection of hydrogen peroxide. *Small* 9, 1703–1707. doi:10.1002/smll.201200683

Chabot, V., Higgins, D., Yu, A., Xiao, X., Chen, Z., and Zhang, J. (2014). A review of graphene and graphene oxide sponge: material synthesis and applications to energy and the environment. *Energy Environ. Sci.* 7, 1564–1596. doi:10.1039/c3ee43385d

Chen, M., Zhang, C., Li, X., Zhang, L., Ma, Y., Zhang, L., et al. (2013a). A one-step method for reduction and self-assembling of graphene oxide into reduced graphene oxide aerogels. *J. Mater. Chem. A* 1, 2869–2877. doi:10.1039/C2TA00820C

Chen, P., Yang, J. J., Li, S. S., Wang, Z., Xiao, T. Y., Qian, Y. H., et al. (2013b). Hydrothermal synthesis of macroscopic nitrogen-doped graphene hydrogels for ultrafast supercapacitor. *Nano Energy* 2, 249–256. doi:10.1016/j.nanoen.2012.09.003

Chen, Q., Hu, Y., Hu, C., Cheng, H., Zhang, Z., Shao, H., et al. (2014). Graphene quantum dots-three dimensional graphene composites for high-performance

supercapacitors. *Phys. Chem. Chem. Phys.* 16, 19307–19313. doi:10.1039/C4CP02761B

Chen, W., Li, S., Chen, C., and Yan, L. (2011a). Self-assembly and embedding of nanoparticles by in situ reduced graphene for preparation of a 3D graphene/nanoparticle aerogel. *Adv. Mater.* 23, 5679–5683. doi:10.1002/adma.201102838

Chen, W., and Yan, L. (2011). In situ self-assembly of mild chemical reduction graphene for three-dimensional architectures. *Nanoscale* 3, 3132–3137. doi:10.1039/C1NR10355E

Chen, Z., Ren, W., Gao, L., Liu, B., Pei, S., and Cheng, H. M. (2011b). Three-dimensional flexible and conductive interconnected graphene networks grown by chemical vapour deposition. *Nat. Mater.* 10, 424–428. doi:10.1038/nmat3001

Cong, H. P., Ren, X. C., Wang, P., and Yu, S. H. (2012). Macroscopic multifunctional graphene-based hydrogels and aerogels by a metal ion induced self-assembly process. *ACS Nano* 6, 2693–2703. doi:10.1021/nn300082k

Dong, X., Wang, J., Wang, J., Park, M. B. C., Li, X., Wang, L., et al. (2012). Supercapacitor electrode based on three-dimensional graphene-polyaniline hybrid. *Mater. Chem. Phys.* 134, 576–580. doi:10.1016/j.matchemphys.2012.03.066

Dong, Y., Liu, S., Wang, Z., Liu, Y., Zhao, Z., and Qiu, J. (2015). Compressible graphene aerogel supported CoO nanostructures as a binder-free electrode for high-performance lithium-ion batteries. *RSC Adv.* 5, 8929–8932. doi:10.1039/C4RA14519D

Estevez, L., Kelarakis, A., Gong, Q., Da'as, E. H., and Giannelis, E. P. (2011). Multifunctional graphene/platinum/nafion hybrids via ice templating. *J. Am. Chem. Soc.* 133, 6122–6125. doi:10.1021/ja200244s

Fang, Q., and Chen, B. (2014). Self-assembly of graphene oxide aerogels by layered double hydroxides cross-linking and their application in water purification. *J. Mater. Chem. A* 2, 8941–8951. doi:10.1039/C4TA00321G

Fang, Q., Shen, Y., and Chen, B. (2015). Synthesis, decoration and properties of three-dimensional graphene-based macrostructures: a review. *Chem. Eng. J.* 264, 753–771. doi:10.1016/j.cej.2014.12.001

Gao, K., Shao, Z., Li, J., Wang, X., Peng, X., Wang, W., et al. (2013). Cellulose nanofiber-graphene all solid state flexible supercapacitors. *J. Mater. Chem. A* 1, 63–67. doi:10.1039/C2TA00386D

Garakani, M. A., Abouali, S., Zhang, B., Takagi, C. A., Xu, Z. L., Huang, J. Q., et al. (2014). Cobalt carbonate/and cobalt oxide/graphene aerogel composite anodes for high performance Li-ion batteries. *ACS Appl. Mater. Interfaces* 6, 18971–18980. doi:10.1021/am504851s

He, Y., Chen, W., Li, X., Zhang, Z., Fu, J., Zhao, C., et al. (2013a). Freestanding three-dimensional graphene/MnO_2 composite networks as ultralight and flexible supercapacitor electrodes. *ACS Nano* 7, 174–182. doi:10.1021/nn304833s

He, Y., Liu, Y., Wu, T., Ma, J., Wang, X., Gong, Q., et al. (2013b). An environmentally friendly method for the fabrication of reduced graphene oxide foam with a super oil absorption capacity. *J. Hazard. Mater.* 260, 796–805. doi:10.1016/j.jhazmat.2013.06.042

Hong, J. Y., Bak, B. M., Wie, J. J., Kong, J., and Park, H. S. (2015). Reversibly compressible, highly elastic, and durable graphene aerogels for energy storage devices under limiting conditions. *Adv. Funct. Mater.* 25, 1053–1062. doi:10.1002/adfm.201403273

Hongxia, B., Ruiyi, L., Zaijun, L., Junkang, L., Zhiguoa, G., and Guanglia, W. (2015). Fabrication of a high density graphene aerogel–gold nanostar hybrid and its application for the electrochemical detection of hydroquinone and *o*-dihydroxybenzene. *RSC Adv.* 5, 54211–54219. doi:10.1039/c5ra06196b

Hu, H., Zhao, Z., Wan, W., Gotosi, Y., and Qiu, J. (2013). Ultralight and highly compressible graphene aerogels. *Adv. Mater.* 25, 2219–2223. doi:10.1002/adma.201204530

Huang, C., Li, C., and Shi, G. (2012). Graphene based catalysts. *Energy Environ. Sci.* 5, 8848–8868. doi:10.1039/C2EE22238H

Jiang, H., Lee, P. S., and Li, C. (2013). 3D carbon based nanostructures for advanced supercapacitors. *Energy Environ. Sci.* 6, 41–53. doi:10.1039/C2EE23284G

Jiang, X., Ma, Y., Li, J., Fan, Q., and Huang, W. (2010). Self-assembly of reduced graphene oxide into three-dimensional architecture by divalent ion linkage. *J. Phys. Chem. C* 114, 22462–22465. doi:10.1021/jp108081g

Jiang, Y., Lu, M., Ling, X., Jiao, Z., Chen, L., Chen, L., et al. (2015). One-step hydrothermal synthesis of three-dimensional porous graphene aerogels/sulfur nanocrystals for lithium–sulfur batteries. *J. Alloys Compd.* 645, 509–516. doi:10.1016/j.jallcom.2015.05.125

Ju, H. F., Song, W. L., and Fan, L. Z. (2014). Rational design of graphene/porous carbon aerogels for high-performance flexible all-solid-state supercapacitors. *J. Mater. Chem. A* 2, 10895–10903. doi:10.1039/C4TA00538D

Juanjuan, Z., Ruiyi, L., Zaijun, L., Junkang, L., Zhiguoa, G., and Guangli, W. (2014). Synthesis of nitrogen-doped activated graphene aerogel/gold nanoparticles and its application for electrochemical detection of hydroquinone and o-dihydroxybenzene. *Nanoscale* 6, 5458–5466. doi:10.1039/c4nr00005f

Jung, S. M., Mafra, D. L., Lin, C. T., Jung, H. Y., and Kong, J. (2015). Controlled porous structures of graphene aerogels and their effect on supercapacitor performance. *Nanoscale* 7, 4386–4393. doi:10.1039/C4NR07564A

Kim, B. J., Yang, G., Park, M. J., Kwak, J. S., Baik, K. H., Kim, D., et al. (2013). Three-dimensional graphene foam-based transparent conductive electrodes in GaN-based blue light-emitting diodes. *Appl. Phys. Lett.* 102, 161902. doi:10.1063/1.4801763

Kuang, J., Liu, L., Gao, Y., Zhou, D., Chen, Z., Han, B., et al. (2013). A hierarchically structured graphene foam and its potential as a large-scale strain-gauge sensor. *Nanoscale* 5, 12171–12177. doi:10.1039/C3NR03379A

Lee, W. S. V., Peng, E., Choy, D. C., and Xue, J. M. (2015). Mechanically robust glucose strutted graphene aerogel paper as a flexible electrode. *J. Mater. Chem. A* 3, 19144–19147. doi:10.1039/C5TA06072A

Lee, Y. J., Park, H. W., Kim, G. P., Yi, J., and Song, I. K. (2013). Supercapacitive electrochemical performance of graphene-containing carbon aerogel prepared using polyethyleneimine-modified graphene oxide. *Curr. Appl. Phys.* 13, 945–949. doi:10.1016/j.cap.2013.02.005

Li, C., Qiu, L., Zhang, B., Li, D., and Liu, C. Y. (2016). Robust vacuum-/air-dried graphene aerogels and fast recoverable shape-memory hybrid foams. *Adv. Mater.* 28, 1510–1516. doi:10.1002/adma.201504317

Li, C., and Shi, G. (2012). Three-dimensional graphene architectures. *Nanoscale* 4, 5549–5563. doi:10.1039/C2NR31467C

Li, D., and Kaner, R. B. (2008). Graphene-based materials. *Science* 320, 1170–1171. doi:10.1126/science.1158180

Li, D., Müller, M. B., Gilje, S., Kaner, R. B., and Wallace, G. G. (2008). Processable aqueous dispersions of graphene nanosheets. *Nat. Nanotechnol.* 3, 101–105. doi:10.1038/nnano.2007.451

Li, J., Li, J., Meng, H., Xie, S., Zhang, B., Li, L., et al. (2014). Ultra-light, compressible and fire-resistant graphene aerogel as a highly efficient and recyclable absorbent for organic liquids. *J. Mater. Chem. A* 2, 2934–2941. doi:10.1039/C3TA14725H

Li, J., Wang, F., and Liu, C. Y. (2012). Tri-isocyanate reinforced graphene aerogel and its use for crude oil adsorption. *J. Colloid Interface Sci.* 382, 13–16. doi:10.1016/j.jcis.2012.05.040

Li, W., Wang, J., Ren, J., and Qu, X. (2013). 3D graphene oxide-polymer hydrogel: near-infrared light-triggered active scaffold for reversible cell capture and on-demand release. *Adv. Mater.* 25, 6737–6743. doi:10.1002/adma.201302810

Li, Z., Wang, J., Liu, S., Liu, X., and Yang, S. (2011). Synthesis of hydrothermally reduced graphene/MnO_2 composites and their electrochemical properties as supercapacitors. *J. Power Sources* 196, 8160–8165. doi:10.1016/j.jpowsour.2011.05.036

Liang, J., Liu, Y., Guo, L., and Li, L. (2013). Facile one-step synthesis of a 3D macroscopic SnO_2-graphene aerogel and its application as a superior anode material for Li-ion batteries. *RSC Adv.* 3, 11489–11492. doi:10.1039/C3RA40873F

Lin, H., Xu, S., Wang, X., and Mei, N. (2013). Significantly reduced thermal diffusivity of free-standing two-layer graphene in graphene foam. *Nanotechnology* 24, 415706. doi:10.1088/0957-4484/24/41/415706

Liu, D., Wang, Y., and Zhao, G. (2015a). Preparation of graphene aerogel for determining oxalic acid. *Int. J. Electrochem. Sci.* 10, 6794–6802.

Liu, J., Cui, L., Kong, N., Barrow, C. J., and Yang, W. (2014). RAFT controlled synthesis of graphene/polymer hydrogel with enhanced mechanical property for pH-controlled drug release. *Eur. Polym. J.* 50, 9–17. doi:10.1016/j.eurpolymj.2013.10.015

Liu, X., Li, H., Zeng, Q., Zhang, Y., Kang, H., Duan, H., et al. (2015b). Electro-active shape memory composites enhanced by flexible carbon nanotube/graphene aerogels. *J. Mater. Chem. A* 3, 11641–11649. doi:10.1039/c5ta02490k

Liu, Y., He, D., Wu, H., Duan, J., and Zhang, Y. (2015c). Hydrothermal self-assembly of manganese dioxide/manganese carbonate/reduced graphene oxide aerogel for asymmetric supercapacitors. *Electrochim. Acta* 164, 154–162. doi:10.1016/j.electacta.2015.01.223

Lo, C. W., Zhu, D., and Jiang, H. (2011). An infrared-light responsive graphene-oxide incorporated poly(N-isopropylacrylamide) hydrogel nanocomposite. *Soft Matter* 7, 5604–5609. doi:10.1039/C1SM00011J

Lv, P., Yu, K., Tan, X., Zheng, R., Ni, Y., Wang, Z., et al. (2016). Super-elastic graphene/carbon nanotube aerogels and their applications as a strain-gauge sensor. *RSC Adv.* 6, 11256–11261. doi:10.1039/C5RA20342B

Maiti, U. N., Lim, J., Lee, K. E., Lee, W. J., and Kim, S. O. (2014). Three-dimensional shape engineered, interfacial gelation of reduced graphene oxide for high rate, large capacity supercapacitors. *Adv. Mater.* 26, 615–619. doi:10.1002/adma.201303503

Menzel, R., Barg, S., Miranda, M., Anthony, D. B., Bawaked, S. M., Mokhtar, M., et al. (2015). Joule heating characteristics of emulsion-templated graphene aerogels. *Adv. Funct. Mater.* 25, 28–35. doi:10.1002/adfm.201401807

Min, Z., Wen-Long, W., and Xue-Dong, B. (2013). Preparing three-dimensional graphene architectures: review of recent developments. *Chin. Phys. B* 22, 098105. doi:10.1088/1674-1056/22/09/098105

Moon, I. K., Yoon, S., Chun, K. Y., and Oh, J. (2015). Highly elastic and conductive N-doped monolithic graphene aerogels for multifunctional applications. *Adv. Funct. Mater.* 25, 6976–6984. doi:10.1002/adfm.201502395

Nardecchia, S., Carriazo, D., Ferrer, M. L., Gutiérrez, M. C., and del Monte, F. (2013). Three dimensional macroporous architectures and aerogels built of carbon nanotubes and/or graphene: synthesis and applications. *Chem. Soc. Rev* 42, 794–830. doi:10.1039/C2CS35353A

Novoselov, K. S., Geim, A. K., Morozov, S. V., Jiang, D., Katsnelson, M. I., Grigorieva, I. V., et al. (2005). Two-dimensional gas of massless Dirac fermions in graphene. *Nature* 438, 197–200. doi:10.1038/nature04233

Nguyen, S. T., Nguyen, H. T., Rinaldi, A., Nguyen, N. P. V., Fan, Z., and Duong, H. M. (2012). Morphology control and thermal stability of binderless-graphene aerogels from graphite for energy storage applications. *Colloids Surf. A* 414, 352–358. doi:10.1016/j.colsurfa.2012.08.048

Qin, S. Y., Liu, X. J., Zhuo, R. X., and Zhang, X. Z. (2012). Microstructure-controllable graphene oxide hydrogel film based on a pH-responsive graphene oxide hydrogel. *Macromol. Chem. Phys.* 213, 2044–2051. doi:10.1002/macp.201200281

Qin, Y., Peng, Q., Ding, Y., Lin, Z., Wang, C., Li, Y., et al. (2015). Lightweight, superelastic, and mechanically flexible graphene/polyimide nanocomposite foam for strain sensor application. *ACS Nano* 9, 8933–8941. doi:10.1021/acsnano.5b02781

Qiu, B., Xing, M., and Zhang, J. (2014a). Mesoporous TiO_2 nanocrystals grown in situ on graphene aerogels for high photocatalysis and lithium-ion batteries. *J. Am. Chem. Soc.* 136, 5852–5855. doi:10.1021/ja500873u

Qiu, L., Liu, D., Wang, Y., Cheng, C., Zhou, K., Ding, J., et al. (2014b). Mechanically robust, electrically conductive and stimuli-responsive binary network hydrogels enabled by superelastic graphene aerogels. *Adv. Mater.* 26, 3333–3337. doi:10.1002/adma.201305359

Qiu, L., Liu, J. Z., Chang, S. L. Y., Wu, Y., and Li, D. (2012). Biomimetic superelastic graphene-based cellular monoliths. *Nat. Commun.* 3, 1241. doi:10.1038/ncomms2251

Ren, L., Hui, K. N., Hui, K. S., Liu, Y., Qi, X., Zhong, J., et al. (2015). 3D hierarchical porous graphene aerogel with tunable meso-pores on graphene nanosheets for high-performance energy storage. *Sci. Rep.* 5, 14229. doi:10.1038/srep14229

Ren, L., Hui, K. S., and Hui, K. N. (2013). Self-assembled free-standing three-dimensional nickel nanoparticle/graphene aerogel for direct ethanol fuel cells. *J. Mater. Chem. A* 1, 5689–5694. doi:10.1039/C3TA10657H

Samad, Y. A., Li, Y., Schiffer, A., Alhassan, S. M., and Liao, K. (2015). Graphene foam developed with a novel two-step technique for low and high strains and pressure-sensing applications. *Small* 11, 2380–2385. doi:10.1002/smll.201403532

Si, W., Wu, X., Zhou, J., Guo, F., Zhuo, S., Cui, H., et al. (2013). Reduced graphene oxide aerogel with high-rate supercapacitive performance in aqueous electrolytes. *Nanoscale Res. Lett.* 8, 247. doi:10.1186/1556-276X-8-247

Stoller, M. D., Park, S., Zhu, Y., An, J., and Ruoff, R. S. (2008). Graphene-based ultracapacitors. *Nano Lett.* 8, 3498–3502. doi:10.1021/nl802558y

Sui, Z. Y., Meng, Y. N., Xiao, P. W., Zhao, Z. Q., Wei, Z. X., and Han, B. H. (2015a). Nitrogen-doped graphene aerogels as efficient supercapacitor electrodes and gas adsorbents. *ACS Appl. Mater. Interfaces* 7, 1431–1438. doi:10.1021/am5042065

Sui, Z. Y., Wang, C., Shu, K., Yang, Q. S., Ge, Y., Wallace, G. G., et al. (2015b). Manganese dioxide-anchored three-dimensional nitrogen doped graphene hybrid aerogels as excellent anode materials for lithium ion batteries. *J. Mater. Chem. A* 3, 10403–10412. doi:10.1039/C5TA01508A

Sui, Z. Y., Wang, C., Yang, Q. S., Shu, K., Liu, Y. W., Han, B. H., et al. (2015c). A highly nitrogen-doped porous graphene – an anode material for lithium ion batteries. *J. Mater. Chem. A* 3, 18229–18237. doi:10.1039/C5TA05759K

Sun, H., Xu, Z., and Gao, G. (2013). Multifunctional, ultra-flyweight, synergistically assembled carbon aerogels. *Adv. Mater.* 25, 2554–2560. doi:10.1002/adma.201204576

Sun, R., Chen, H., Li, Q., Song, Q., and Zhang, X. (2014). Spontaneous assembly of strong and conductive graphene/polypyrrole hybrid aerogels for energy storage. *Nanoscale* 6, 12912–12920. doi:10.1039/C4NR03322A

Sun, X., Cheng, P., Wang, H., Xu, H., Dang, L., Liu, Z., et al. (2015). Activation of graphene aerogel with phosphoric acid for enhanced electrocapacitive performance. *Carbon N. Y.* 92, 1–10. doi:10.1016/j.carbon.2015.02.052

Tai, Z., Yan, X., and Xue, Q. (2012). Three-dimensional graphene/polyaniline composite hydrogel as supercapacitor electrode. *J. Electrochem. Soc.* 159, A1702–A1709. doi:10.1149/2.058210jes

Tan, C., Cao, J., Khattak, A. M., Cai, F., Jiang, B., Yang, G., et al. (2014). High-performance tin oxide-nitrogen doped graphene aerogel hybrids as anode materials for lithium-ion batteries. *J. Power Sources* 270, 28–33. doi:10.1016/j.jpowsour.2014.07.059

Tang, M., Wu, T., Na, H., Zhang, S., Li, X., and Pang, X. (2015). Fabrication of graphene oxide aerogels loaded with catalytic AuPd nanoparticles. *Mater. Res. Bull.* 63, 248–252. doi:10.1016/j.materresbull.2014.12.008

Tang, Z., Shen, S., Zhuang, J., and Wang, X. (2010). Noble-metal-promoted three-dimensional macroassembly of single-layered graphene oxide. *Angew. Chem. Int. Ed.* 49, 4603–4607. doi:10.1002/anie.201000270

Trung, N. B., Tam, T. V., Kim, H. R., Hur, S. H., Kim, E. J., and Choi, W. M. (2014). Three-dimensional hollow balls of graphene–polyaniline hybrids for supercapacitor applications. *Chem. Eng. J.* 255, 89–96. doi:10.1016/j.cej.2014.06.028

Vickery, J. L., Patil, A. J., and Mann, S. (2009). Fabrication of graphene-polymer nanocomposites with higher-order three-dimensional architectures. *Adv. Mater.* 21, 2180–2184. doi:10.1002/adma.200803606

Wang, B., Abdulla, W. A., Wang, D., and Zhao, X. S. (2015a). A three-dimensional porous LiFePO4 cathode material modified with a nitrogen-doped graphene aerogel for high-power lithium ion batteries. *Energy Environ. Sci.* 8, 869–875. doi:10.1039/C4EE03825H

Wang, B., Yan, S., and Shi, Y. (2015b). Direct electrochemical analysis of glucose oxidase on a graphene aerogel/gold nanoparticle hybrid for glucose biosensing. *J. Solid State Electrochem.* 19, 307–314. doi:10.1007/s10008-014-2608-7

Wang, C. C., Chen, H. C., and Lu, S. Y. (2013a). Manganese oxide/graphene aerogel composites as an outstanding supercapacitor electrode material. *Chem. Eur. J.* 20, 517–523. doi:10.1002/chem.201303483

Wang, E., Desai, M. S., and Lee, S. W. (2013b). Light-controlled graphene-elastin composite hydrogel actuators. *Nano Lett.* 13, 2826–2830. doi:10.1021/nl401088b

Wang, H., Zhang, D., Yan, T., Wen, X., Zhang, J., Shi, L., et al. (2013c). Three-dimensional macroporous graphene architectures as high performance electrodes for capacitive deionization. *J. Mater. Chem. A* 1, 11778–11789. doi:10.1039/C3TA11926B

Wang, R., Xu, C., Sun, J., Gao, L., and Yao, H. (2014). Solvothermal-induced 3D macroscopic SnO_2/nitrogen-doped graphene aerogels for high capacity and long-life lithium storage. *ACS Appl. Mater. Interfaces* 6, 3427–3436. doi:10.1021/am405557c

Wei, W., Yang, S., Zhou, H., Lieberwirth, I., Feng, X., and Müllen, K. (2013). 3D graphene foams cross-linked with pre-encapsulated Fe_3O_4 nanospheres for enhanced lithium storage. *Adv. Mater.* 25, 2909–2914. doi:10.1002/adma.201300445

Worsley, M. A., Pauzauskie, P. J., Olson, T. Y., Biener, J., Satcher, J. H., and Baumann, T. F. (2010). Synthesis of graphene aerogel with high electrical conductivity. *J. Am. Chem. Soc.* 132, 14067–14069. doi:10.1021/ja1072299

Wu, X., Zhou, J., Xing, W., Wang, G., Cui, H., Zhuo, S., et al. (2012a). High-rate capacitive performance of graphene aerogel with a superhigh C/O molar ratio. *J. Mater. Chem.* 22, 23186–23193. doi:10.1039/C2JM35278H

Wu, Y., Gao, G., and Wu, G. (2015a). Self-assembled three-dimensional hierarchical porous V_2O_5/graphene hybrid aerogels for supercapacitors with high energy density and long cycle life. *J. Mater. Chem. A* 3, 1828–1832. doi:10.1039/C4TA05537C

Wu, Y., Yi, N., Huang, L., Zhang, T., Fang, S., Chang, H., et al. (2015b). Three-dimensionally bonded spongy graphene material with super compressive elasticity and near-zero Poisson's ratio. *Nat. Commun.* 6, 6141. doi:10.1038/ncomms7141

Wu, Z. S., Sun, Y., Tan, Y. Z., Yang, S., Feng, X., and Müllen, K. (2012b). Three-dimensional graphene-based macro- and mesoporous frameworks for high-performance electrochemical capacitive energy storage. *J. Am. Chem. Soc.* 134, 19532–19535. doi:10.1021/ja308676h

Wu, Z. S., Winter, A., Chen, L., Sun, Y., Turchanin, A., Feng, X., et al. (2012c). Three-dimensional nitrogen and boron co-doped graphene for high-performance

all-solid-state supercapacitors. *Adv. Mater.* 24, 5130–5135. doi:10.1002/adma.201201948

Wu, Z. S., Yang, S., Sun, Y., Parvez, K., Feng, X., and Müllen, K. (2012d). 3D nitrogen-doped graphene aerogel-supported Fe_3O_4 nanoparticles as efficient electrocatalysts for the oxygen reduction reaction. *J. Am. Chem. Soc.* 134, 9082–9085. doi:10.1021/ja3030565

Xiao, L., Wu, D., Han, S., Huang, Y., Li, S., He, M., et al. (2013). Self-assembled Fe_2O_3/graphene aerogel with high lithium storage. *ACS App. Mater. Interfaces* 5, 3764–3769. doi:10.1021/am400387t

Xiao, X., Beechem, T. E., Brumbach, M. T., Lambert, T. N., Davis, D. J., Michael, J. R., et al. (2012). Lithographically defined three-dimensional graphene structures. *ACS Nano* 6, 3573–3579. doi:10.1021/nn300655c

Xie, X., Zhou, Y., Bi, H., Yin, K., Wan, S., and Sun, L. (2013). Large-range control of the microstructures and properties of three-dimensional porous graphene. *Sci. Rep.* 3, 2117. doi:10.1038/srep02117

Xie, Y., Meng, Z., Cai, T., and Han, W. Q. (2015). Effect of boron-doping on the graphene aerogel used as cathode for the lithium–sulfur battery. *ACS Appl. Mater. Interfaces* 7, 25202–25210. doi:10.1021/acsami.5b08129

Xu, L., Xiao, G., Chen, C., Run, L., Mai, Y., Sun, G., et al. (2015a). Superhydrophobic and superoleophilic graphene aerogel prepared by facile chemical reduction. *J. Mater. Chem. A* 3, 7498–7504. doi:10.1039/C5TA00383K

Xu, X., Li, H., Zhang, Q., Hu, H., Zhao, Z., Li, J., et al. (2015b). Self-sensing, ultralight, and conductive 3D graphene/iron oxide aerogel elastomer deformable in a magnetic field. *ACS Nano* 9, 3969–3977. doi:10.1021/nn507426u

Xu, Y., Sheng, K., Li, C., and Shi, G. (2010). Self-assembled graphene hydrogel via a one-step hydrothermal process. *ACS Nano* 4, 4324–4330. doi:10.1021/nn101187z

Yan, X., Yao, W., Hu, L., Liu, D., Wang, C., and Lee, C. S. (2015). Progress in the preparation and application of three-dimensional graphene-based porous nanocomposites. *Nanoscale* 7, 5563–5577. doi:10.1039/C5NR00030K

Yang, F., Xu, M., Bao, S. J., Wei, H., and Chai, H. (2014). Self-assembled hierarchical graphene/polyaniline hybrid aerogels for electrochemical capacitive energy storage. *Electrochim. Acta* 137, 381–387. doi:10.1016/j.electacta.2014.06.017

Yang, S., Zhang, L., Yang, Q., Zhang, Z., Chen, B., Lv, P., et al. (2015). Graphene aerogel prepared by thermal evaporation of graphene oxide suspension containing sodium bicarbonate. *J. Mater. Chem. A* 3, 7950–7958. doi:10.1039/C5TA01222H

Yao, X., Guo, G., Ma, X., Zhao, Y., Ang, C. Y., Luo, Z., et al. (2015). In situ integration of anisotropic SnO_2 heterostructures inside three-dimensional graphene aerogel for enhanced lithium storage. *ACS Appl. Mater. Interfaces* 7, 26085–26093. doi:10.1021/acsami.5b07081

Yavari, F., Chen, Z., Thomas, A. V., Ren, W., Cheng, H. M., and Koratkar, N. (2011). High sensitivity gas detection using a macroscopic three-dimensional graphene foam network. *Sci. Rep.* 1, 166. doi:10.1038/srep00166

Ye, S., and Feng, J. (2014). Self-assembled three-dimensional hierarchical graphene/polypyrrole nanotube hybrid aerogel and its application for supercapacitors. *ACS Appl. Mater. Interfaces* 6, 9671–9679. doi:10.1021/am502077p

Ye, S., Feng, J., and Wu, P. (2013). Deposition of three-dimensional graphene aerogel on nickel foam as a binder-free supercapacitor electrode. *ACS Appl. Mater. Interfaces* 5, 7122–7129. doi:10.1021/am401458x

Yong, Y. C., Dong, X. C., Park, M. B. C., Song, H., and Chen, P. (2012). Macroporous and monolithic anode based on polyaniline hybridized three-dimensional graphene for high-performance microbial fuel cells. *ACS Nano* 6, 2394–2400. doi:10.1021/nn204656d

Yu, G., Hu, L., Vosgueritchian, M., Wang, H., Xie, X., McDonough, J. R., et al. (2011). Solution-processed graphene/MnO_2 nanostructured textiles for high-performance electrochemical capacitors. *Nano Lett.* 11, 2905–2911. doi:10.1021/nl2013828

Yu, X., Park, S. K., Yeon, S. H., and Park, H. S. (2015a). Three-dimensional, sulfur-incorporated graphene aerogels for the enhanced performances of pseudocapacitive electrodes. *J. Power Sources* 278, 484–489. doi:10.1016/j.jpowsour.2014.12.102

Yu, Z., Mclnnis, M., Calderon, J., Seal, S., Lei, Z., and Thomas, J. (2015b). Functionalized graphene aerogel composites for high-performance asymmetric supercapacitors. *Nano Energy* 11, 611–620. doi:10.1016/j.nanoen.2014.11.030

Zhai, Y., Dou, Y., Zhao, D., Fulvio, P. F., Mayes, R. T., and Dai, S. (2011). Carbon materials for chemical capacitive energy storage. *Adv. Mater.* 23, 4828–4850. doi:10.1002/adma.201100984

Zhang, L., Chen, G., Hedhili, M. N., Zhang, H., and Wang, P. (2012). Three-dimensional assemblies of graphene prepared by a novel chemical reduction-induced self-assembly method. *Nanoscale* 4, 7038–7045. doi:10.1039/C2NR32157B

Zhang, X., Sui, Z., Xu, B., Yue, S., Luo, Y., Zhan, W., et al. (2011). Mechanically strong and highly conductive graphene aerogel and its use as electrodes for electrochemical power sources. *J. Mater. Chem.* 21, 6494–6497. doi:10.1039/C1JM10239G

Zhao, Y., Hu, C., Hu, Y., Cheng, H., Shi, G., and Qu, L. (2012a). A versatile, ultralight, nitrogen-doped graphene framework. *Angew. Chem.* 124, 11533–11537. doi:10.1002/ange.201206554

Zhao, Y., Liu, J., Hu, Y., Cheng, H., Hu, C., Jiang, C., et al. (2012b). Highly compression-tolerant supercapacitor based on polypyrrole-mediated graphene foam electrodes. *Adv. Mater.* 25, 591–595. doi:10.1002/adma.201203578

Zhong, C., Wang, J. Z., Gao, X. W., Wexler, D., and Liu, H. K. (2013). *In situ* one-step synthesis of a 3D nanostructured germanium-graphene composite and its application in lithium-ion batteries. *J. Mater. Chem. A* 1, 10798–10804. doi:10.1039/C3TA11796K

Zhou, G., Li, F., and Cheng, H. M. (2014). Progress in flexible lithium batteries and future prospects. *Energy Environ. Sci.* 7, 1307–1338. doi:10.1039/C3EE43182G

Zhu, C., Han, Y. J., Duoss, E. B., Golobic, A. M., Kuntz, J. D., Spadaccini, C. M., et al. (2015). Highly compressible 3D periodic graphene aerogel microlattices. *Nat. Commun* 6, 6962. doi:10.1038/ncomms7962

Zhu, Y., Li, L., Zhang, C., Casillas, G., Sun, Z., Yan, Z., et al. (2012). A seamless three-dimensional carbon nanotube graphene hybrid material. *Nat. Commun.* 3, 1225. doi:10.1038/ncomms2234

Zhu, Y., Murali, S., Stoller, M. D., Ganesh, K. J., Cai, W., Ferreira, P. J., et al. (2011). Carbon-based supercapacitors produced by activation of graphene. *Science* 332, 1537–1541. doi:10.1126/science.1200770

Zou, J., and Kim, F. (2014). Diffusion driven layer-by-layer assembly of graphene oxide nanosheets into porous three-dimensional macrostrucures. *Nat. Commun.* 5, 5254. doi:10.1038/ncomms6254

Conflict of Interest Statement: The authors declare that the research was conducted in the absence of any commercial or financial relationships that could be construed as a potential conflict of interest.